ARL 70-0002
JANUARY 1970

Aerospace Research Laboratories

THEORETICAL AND EXPERIMENTAL STUDIES OF THE SHOCK WAVE-BOUNDARY LAYER INTERACTION ON COMPRESSION SURFACES IN HYPERSONIC FLOW

M. S. HOLDEN
J. R. MOSELLE
CORNELL AERONAUTICAL LABORATORY, INC.
BUFFALO, NEW YORK

Contract No. F33615-67-C-1298
Project No. 7064

OFFICE OF AEROSPACE RESEARCH
United States Air Force

16

NOTICES

When Government drawings, specifications, or other data are used for any purpose other than in connection with a definitely related Government procurement operation, the United States Government thereby incurs no responsibility nor any obligation whatsoever, and the fact that the Government may have formulated, furnished, or in any way supplied the said drawings, specifications, or other data, is not to be regarded by implication or otherwise as in any manner licensing the holder or any other person or corporation, or conveying any rights or permission to manufacture, use, or sell any patented invention that may in any way be related thereto.

Agencies of the Department of Defense, qualified contractors and other government agencies may obtain copies from the

Defense Documentation Center
Cameron Station
Alexandria, Virginia 22314

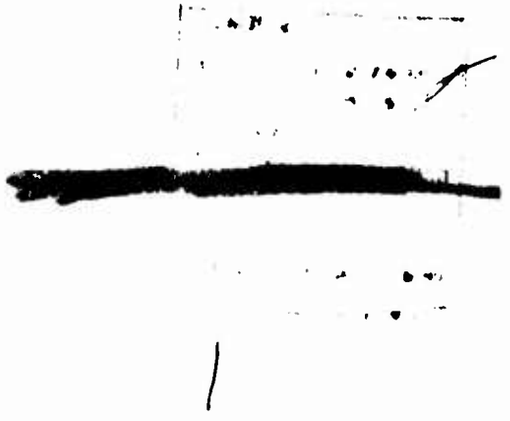

Copies of ARL Technical Documentary Reports should not be returned to Aerospace Research Laboratories unless return is required by security considerations, contractual obligations or notices on a specified document.

300 - April 1970 - CO455 - 113-2478

ARL 70-0002

THEORETICAL AND EXPERIMENTAL STUDIES OF THE SHOCK WAVE-BOUNDARY LAYER INTERACTION ON COMPRESSION SURFACES IN HYPERSONIC FLOW

M. S. HOLDEN and J. R. MOSELLE
CORNELL AERONAUTICAL LABORATORY, INC.
BUFFALO, NEW YORK

JANUARY 1970

Contract No. F33615-67-C-1298
Project No. 7064

AEROSPACE RESEARCH LABORATORIES
OFFICE OF AEROSPACE RESEARCH
UNITED STATES AIR FORCE
WRIGHT-PATTERSON AIR FORCE BASE, OHIO

FOREWORD

The work described in this report was supported by the U. S. Air Force through the Hypersonic Research Laboratory, Aerospace Research Laboratories, Office of Aerospace Research, Wright-Patterson AFB Ohio, under Contract F 33615-67-C-1298. The contract monitor for this program, conducted during the period November 1966 through November 1969 was Dr. Wilbur Hankey. A summary of the studies conducted under this contract is given in the following section. A detailed description is then given of the theoretical and experimental studies of shock wave - laminar boundary layer interaction on curved compression surfaces in hypersonic flow.

The author wishes to acknowledge the contribution of Mr. J. R. Moselle who constructed the IBM machine code used in the theoretical study. The assistance and cooperation of Mr. T. J. Bell and Mr. R. F. Hathaway, of the Hypersonic Facilities Department of CAL, in the experimental program is also gratefully acknowledged.

ABSTRACT

The report first summarizes the studies conducted under this contract. A detailed description is then given of the theoretical and experimental studies of shock wave-laminar boundary layer interaction on curved compression surfaces in hypersonic flow. In the theoretical study we have used the integral forms of the boundary layer equations for the conservation of mass, streamwise momentum, normal momentum, moment of streamwise momentum and energy to describe the development of attached and separated boundary layers on a curve surface. In this formulation we do not assume the pressure to be constant across the boundary layer. The theory, which was in good agreement with measurements on compression surfaces in Mach 10 and 14.8 airflows, showed that large pressure gradients can be generated across the boundary layer in the separation and reattachment regions. In the experimental study, skin friction, heat transfer and pressure measurements were made on a series of flat plate-cylindrical arc-wedge compression surfaces. Pitot and cone pressure measurements were made above the surface in the separation and reattachment regions of separated flows to estimate the static pressure difference across the boundary layer. The radius of curvature of the cylindrical arc, the inclination of the wedge, and the unit Reynolds number of the free-stream were varied to examine their effect on the properties of both attached and separated interaction regions over the models. We found that separation first occurred on the compression surface downstream of the flat plate, and incipient separation could not always be detected by observing the first occurrence of an inflexion point in the pressure distribution. The conditions under which incipient separation occurs were far less sensitive to surface curvature than those observed in earlier experimental studies.

A SUMMARY OF THE RESEARCH PROGRAM

The research program which has been completed at CAL under Contract No. F 33615-67-C-1298 has been devoted to studies of the structure and development of attached and separated boundary layers on compression surfaces in hypersonic flow. The emphasis in this study was placed on examining shock wave-laminar boundary layer interaction at free stream conditions for which laminar boundary layers could be expected to be encountered on high performance maneuverable vehicles. Only on high Mach number flight ($M_\infty > 14$) at high altitudes (low Reynolds numbers) on highly cooled bodies (T_w/T_o, $O(0.1)$) are laminar boundary layers of practical importance. Under these circumstances the interaction between the viscous and inviscid flow over the leading edge (the boundary layer displacement effect) is important; and since the leading edge must be blunt to prevent a large heating load, the effect of the highly non-uniform inviscid flow field (the entropy layer) generated by bluntness must be examined. In many cases the compression surfaces on hypersonic vehicles would be curved and flared into the main body to prevent flow separation, and thus we set out to find how surface curvature affects the development and separation of the boundary layer, and how large are the normal pressure gradients developed across the thick, highly curved boundary layers in these high Mach number flows.

A paper describing the theoretical and experimental study of leading edge bluntness and boundary layer displacement effects on attached and separated laminar boundary layers [29] was presented at the AIAA 6th Aerospace Sciences Meeting in New York (AIAA Paper 68-68), and is to be published in two parts in the AIAA journal. A paper describing the theoretical and experimental studies of the shock wave-boundary layer interaction on curved compression surfaces was presented at the symposium on "Viscous Interaction Phenomena in Supersonic and Hypersonic Flow" sponsored by the Hypersonic Research Laboratory of the Aerospace Research Laboratories, Wright-Patterson Air Force Base, Ohio,

10-13 May 1969. This latter work is described in full in this report.

Leading-Edge Bluntness and Boundary Layer Displacement Effects

In this work we made a detailed theoretical and experimental study of the problem. The theoretical analysis used the integral forms of the boundary layer equations for the conservation of mass, momentum, moment of momentum and energy to describe the development of the viscous layer and its interaction with the outer inviscid flow. The analysis was based on a method successfully developed earlier to describe shock-induced separated flow with large wall cooling,but applicable only to situations where the interaction upstream of the corner was weak. Here we studied flows in which the pressure gradient developed by the viscous-inviscid interaction over the basic flat plate was strong and in which there is a strong interaction between the viscous and inviscid flow in the corner interaction region.

For flows over highly cooled flat plates in the strong interaction regime, the analysis indicated that the boundary layer became supercritical; i.e., it will thin when subjected to an adverse pressure gradient. In this formulation of the problem,in order to join the solution of the boundary layer equation close to the separation point (where the boundary layer is subcritical) to the integration at the beginning of the interaction, it is necessary to make a small but finite jump from the supercritical to the subcritical branch of the solution. Here, the strength of this jump is specified by satisfying the conservation of mass, momentum, moment of momentum and energy across the jump. Good agreement has been found between theory and experiment throughout the interaction region for highly cooled flows in the weak interaction regime.

In the strong interaction regime we found good agreement between theory and experiment. However, in this case, we experienced difficulty in integrating smoothly through the neck region of the flow, and we had to introduce a scale length from the experimental study to specify a unique solution. At this time it was believed this problem arose because the pressure gradient developed normal to the viscous layer was

neglected in the formulation of the analysis. Indeed, this was found to be the case, for in the analysis which we developed subsequently in which the normal pressure gradient was taken into account, we experienced no problems in integrating smoothly through the neck region.

The experimental investigation of leading edge bluntness and boundary layer displacement effects on attached and separated flows over compression surfaces was one of the first systematic and detailed studies to be made of this problem. For the first time simultaneous measurements of skin friction, heat transfer and pressure were made, together with schlieren photographs of the flows on a series of sharp and blunt flat plate-wedge compression surfaces over a range of free stream Reynolds numbers and Mach numbers. As in earlier studies, we investigated the time required to establish a steady separated flow and the effect of a finite model span on the size and properties of the corner interaction. It was found that, for the range of free-stream conditions and model configurations studied, attached interaction regions were established within the starting time of the tunnel (less than 1 millisecond). However, we found that separated regions could take as long as 2.5 milliseconds to stabilize, and the mechanism of flow establishment was consistent with the propagation of an acoustic disturbance close to the wall. The effect of finite model span on the properties of both attached and separated regions was investigated by varying the model span while monitoring both the longitudinal and spanwise properties on the model. Although increasing the model span from 1 ft to 1.5 ft did not measurably influence the properties of the attached interaction regions, it did cause a small increase in the size of large separated regions. However, further increasing the model span to 2 ft had little additional effect, and the addition of side fences to this latter configuration did not affect the flow. It was found that a uniform distribution of properties across the center span of the model does not necessarily imply that the measurements are free from span effects. Also, side fences should be used with care, for their addition to some configurations can cause as much flow distortion as the lack of them.

In the experimental studies of shock wave-boundary layer interaction on the highly cooled sharp flat plate-wedge models, which was performed at Mach numbers from 14 to 20 and unit Reynolds numbers for 2200/in to 14,000/in, we found that the upstream influence on the wedge in attached flows was extremely small. However, when separation is promoted, the interaction feeds forward very rapidly as the wedge angle is increased. The abrupt change in the extent of the upstream influence is in marked contrast with the character of laminar boundary layers in supersonic flow where the upstream influence increases uniformly with wedge angle in both attached and separated flows. The length of the separated region was found to decrease with increasing free stream Mach number and decreasing unit Reynolds number. A plateau pressure region was found in all well separated flows, and the plateau pressure ratio was correlated in terms of $\chi_{\epsilon_L}^{1/2}$. The incipient separation condition was determined at each free stream condition from the skin friction, heat transfer and pressure measurements. The skin friction measurements verified the separation criteria, based on characteristic changes in the form of the heat transfer and pressure distributions with wedge angle, which had been proposed in earlier studies. We found that these measurements of the incipient separation condition correlated in the form $M\theta_{incip} = 4.3\chi_{\epsilon_L}^{1/2}$.

The study of the interaction regions on the blunted flat plate-wedge was performed at a free stream Mach number of 19.8 and unit Reynolds numbers of 8700/in and 2055/in for a series of leading edge thicknesses (from 0.007 to 1.2 inches) and shapes (cylindrical and flat) to obtain conditions on the basic flat plate from the viscous to the bluntness-dominated regime ($0.08 < \chi_\epsilon/K_\epsilon^{2/3} < 2$). The measurements of skin friction, heat transfer, and pressure made in the attached flow over the blunted flat plates agree well with the theory of Cheng et al[39] from the displacement to the bluntness-dominated regime ($2 > \chi_\epsilon/K_\epsilon^{2/3} > 0.08$). For well separated flows, increasing the leading edge bluntness for $\chi_\epsilon/K_\epsilon^{2/3} > 0.5$ slightly increased the size of the separated region, whereas for $\chi_\epsilon/K_\epsilon^{2/3} < 0.5$, an increase in the bluntness caused a marked decrease in the length of the separated flow. A well separated region in these flows was always

characterized by a plateau pressure region. The plateau pressure ratio decreased with increased bluntness, and it was found that the measurements correlated in the form $p_{plateau} / p_0 \left(\frac{K_{\epsilon_0}}{\chi_{\epsilon_0}^2}\right)^2$ versus $\chi_{\epsilon_0} / K_\epsilon^{2/3}$. The pressure, heat transfer, and skin friction on the wedge in both attached and separated flows are markedly reduced by leading edge bluntness. Thus, in the design of compression surfaces, a compromise must be reached between protecting the leading edge and recovering as much pressure as possible on the ramp. We found that in flows strongly influenced by leading edge bluntness, the skin friction measurements were the only accurate method of determining incipient separation, though the heat-transfer measurements still provided a qualitative separation criterion. The wedge angle required to cause incipient separation was reduced by leading edge bluntness, though the trend was weak; the measurements correlated in the form $M\theta_{incip}\left(\frac{K_{\epsilon_L}}{\chi_{\epsilon_L}^2}\right) = 4.34\left(\frac{\chi_\epsilon}{K_\epsilon^{2/3}}\right)^{-7/5}$.

A Solution to the Second Order Boundary Layer Equations Including Normal Pressure Gradient

In order to describe properly the viscous-inviscid interaction in the separation and reattachment regions of separated flow in high Mach number, low Reynolds number flows, it is necessary to include the pressure variation across the boundary layer in the formulation of the mathematical model. If the effect of surface curvature on the development and separation of a boundary layer on a curved surface is to be calculated, then the normal momentum equation must be solved simultaneously with the conservation equations in the streamwise direction. In this new theoretical analysis we have derived a model to describe the viscous-inviscid interaction for attached and separated flows over two-dimensional curved compression surfaces in hypersonic flow. Here we have obtained simultaneous solutions to the integral forms of the boundary layer equations for the conservation of mass, streamwise momentum, moment of streamwise momentum, normal momentum and energy. Because the formulation of the analysis was an order of magnitude more difficult than the earlier analysis, we had to use both Cohen and Reshotko solutions and quartic polynomials to describe the velocity and enthalpy profiles. We found

that initial response of the boundary layer to a streamwise pressure gradient at the beginning of the interaction region. Small values of the parameter $\frac{p_w - p_e}{p_w}$ can change the response from supercritical to subcritical. Comparisons among the new analysis, the earlier analysis where $\partial p/\partial y = 0$, and the experimental measurements showed that introducing the normal pressure gradient gave larger streamwise pressure gradients in the separation and reattachment regions, which was in closer agreement with experiment. We did not encounter any problems with the integration in the neck region, which was the area where the theory with $\partial p/\partial y = 0$ broke down in the strong interaction regime. The calculations for this condition were in good agreement with measurements from the experimental program. The calculations indicated that pressure ratios p_w/p_e of the order of 1.6 are generated in the separation and reattachment regions of the flow.

The Experimental Study of Shock Wave-Boundary Layer Interaction on Curved Compression Surfaces

In this study, skin friction, heat transfer and pressure measurements were made on a series of flat plate-cylindrical arc-wedge compression surfaces to examine the effects of radius of curvature on the occurrence and structure of separated regions. Pitot and cone pressure traverses were also made to obtain an estimate of the pressure gradients normal to the surface in the separation and reattachment regions. In these flows, the first indication that flow separation was to occur was provided by the skin friction measurements on the compression surface; the skin friction was first observed to be negative on the surface downstream of the flat plate. On the compression surfaces with large radii of curvature, the incipient separation condition could not be detected with any accuracy by observing the first occurrence of an inflexion point in the pressure distribution or a change in the form of the heat transfer distribution. The static pressure distributions, evaluated from the pitot and cone pressure measurements across the boundary layers in the separation and reattachment regions, indicated that the normal pressure gradients were of the same magnitude as those in the streamwise direction. Although

the experiments were conducted for a range of ratios of δ_o/R, which were similar to those used by Kuehn,[4] and Sterrett and Emery,[5] we found that incipient separation was far less sensitive to surface curvature than indicated in these earlier studies. This we believe results from the structure of the laminar boundary layer in hypersonic flow over highly cooled walls where the streamwise distances for a surface disturbance to propagate to the edge of the boundary layer (where most of the momentum is concentrated) are greater than the length of the curved surface. The measurements were correlated in the form $M_\infty \theta_{incip}$ versus $\bar{\chi}_L^{1/2}\left(1+\frac{Re_R}{Re_\theta}\right)$.

TABLE OF CONTENTS

LIST OF ILLUSTRATIONS

SYMBOLS

$A(X)$ = polynomial velocity profile parameter $\left.\frac{\partial(U/U_e)}{\partial(Y/\delta_i)}\right|_w$

$a(X)$ = velocity profile parameters of Cohen and Reshotko profiles $\frac{\partial(U/U_e)}{\partial Y/\delta_i}$ in attached flow, Y^*/δ_i in separated flow

a_e, a_∞ = speed of sound

$B(X)$ = polynomial total enthalpy profile parameter $\left.\frac{\partial(S/S_w)}{\partial(Y/\delta_i)}\right|_w$

$b(X)$ = total enthalpy parameters of Cohen and Reshotko profiles $\left.\frac{\partial(S/S_w)}{\partial \eta_{CR}}\right|_w$

C = constant in the equation $\frac{\mu}{\mu_\infty} = C\,\frac{T}{T_\infty}$

c = $(p_w - p_e/p_w)$ the pressure profile parameter

c_j = coefficients of the integral forms of the boundary layer equations (see Section 2.3)

c_p, c_v = specific of the gas at constant pressure and volume, respectively

c_H = $\frac{q}{\rho_\infty u_\infty (H_s - H_w)}$

c_F = $\frac{\tau}{\frac{1}{2}\rho_\infty u_\infty^2}$

c_p = $\frac{p}{\rho_\infty u_\infty^2}$

D_j = coefficients of the integral forms of the boundary layer equations (see Section 2.3)

α = $\left(\frac{1+m_e}{m_e}\right)$

f' = $\frac{U}{U_e}$

h = static enthalpy

H, h_s = total and stagnation enthalpy

L = length of flat plate

M = Mach number

m = $\frac{\gamma-1}{2} M^2$

P = $\frac{\delta_i^*}{U_e}\left(\frac{\partial U}{\partial Y}\right)_w$

$P_{1,2,3,\text{ etc}}$ = integral variables from the polynomial profiles (see Appendix)

Pr = Prandtl number

p = static pressure

Q = $\delta_i^* \left(\frac{\partial S/S_w}{\partial Y}\right)_w$

q = heat transfer rate

Re_x = Reynolds number $\frac{\rho_e U_e x}{\mu_e}$

R = radius of surface curvature

S = $\frac{H}{H_e} - 1$

T = $\frac{1}{\delta_i^*}\int_0^{\delta_i} \frac{S}{S_w} \frac{U}{U_e}\, dY$

t = $\frac{1}{\delta_i^*}\int_0^{\delta_i} \frac{S}{S_w}\, dY$

U, V = velocities in the transform plane parallel and normal to the surface, respectively

u, v = velocities parallel and normal to the surface, respectively

W = $\frac{1}{\delta_i}\int_0^{\delta_i} \frac{U}{U_e}\, dY$

X = distance along the surface in the transform plane where $dX = \frac{\rho_e a_e}{\rho_\infty a_\infty}\, dx$

x = distance along the surface

y = distance normal to the surface

Y = distance normal to the surface in the transform plane $dY = \frac{\rho a_e}{\rho_\infty a_\infty}\, dy$

Y^* = distance to the point of zero velocity in a separated shear layer

α = inclination of the surface to the x-axis

β = the Cohen and Reshotko pressure gradient parameter

γ = c_p/c_v

δ = boundary layer thickness

δ^* = displacement thickness

δ_R = $\delta_i^*/\delta_{i_\infty}^*$

ϵ = $(\gamma+1/\gamma-1)$

η = Y/δ_i

η_{CR} = $Y\left[\frac{\bar{m}+1}{2}\ \frac{U_e}{\nu_e x}\right]^{1/2}$

θ = angle of the streamline relative to the x- axis

θ = angle of the streamline relative to the X-axis

θ_w, θ_{incip} = ramp angle, and ramp angle to promote incipient separation

K = surface curvature

μ = viscosity

ν = Prandtl-Meyer function

ρ = density

τ = shear stress

$\bar{\chi}_L$ = viscous interaction parameter $M^3\sqrt{C^*}/Re_L$

ψ = stream function $\left(\int_0^y \frac{\rho u}{\rho_\infty}\, dy\right)$

Subscripts

b = Blasius

CR = based on the Cohen and Reshotko profiles

e = conditions at the edge of the boundary layer

i = conditions in the transform plane

$incip$ = conditions at incipient separation

L	=	based on length of flat plate
o	=	conditions at the beginning of the interaction
p	=	based on the quartic profiles
$plateau$	=	conditions in the constant pressure region of a separated flow
S	=	stagnation conditions
w	=	conditions at the wall
$*$	=	based on the reference temperature $T_* = \frac{T_S}{6}\left[1 + \frac{T_W}{T_S}\right]$
∞	=	free stream conditions

1. INTRODUCTION

The study of the non-similar development of a boundary layer in a strong favorable or adverse pressure gradient has provided one of the more challenging areas of research since the formulation of the boundary layer theory. While most theoretical methods for predicting the structure and development of boundary layers are based on the assumption that the velocity profiles develop in a similar or locally similar fashion, the development of boundary layers in separated flows over bodies or in their near wake can be described only by methods which model the non-similar nature of the flow mechanics inherent in such regions. Within the past decade this subject has received considerable attention because of its importance to the design of compression surfaces on high speed vehicles and the characteristics of the wake of re-entry vehicles. Although many experimental and theoretical studies of laminar and turbulent separated regions have been conducted, the understanding of the basic fluid mechanics is far from complete. However, in one area, that of laminar separated flows caused by shock wave-boundary layer interaction in supersonic flow, theoretical analyses based on solutions to the integral forms of the conventional boundary layer equations have been successful in predicting many of the characteristics observed in experimental studies of these regions.

In most practical situations regions of shock wave-boundary layer interaction are turbulent in supersonic flight; however, in hypersonic flows at high altitudes, fully laminar separated regions exist in continuum flow. In the high Mach number, low Reynolds number regime, where laminar regions of shock wave-boundary layer interaction are of practical importance, some of the basic assumptions made in the theoretical methods successful in predicting the characteristics of such regions in supersonic flow are invalid. In this section we will discuss some fundamental features of these theoretical models and where they can be changed to describe regions of shock wave-laminar boundary layer interaction in high Mach number, low Reynolds number flows over highly cooled curved compression surfaces.

Within the past few years theoretical methods based on solutions to the integral forms of the boundary layer equations[1-10] and finite difference solutions[11-15] of the boundary layer equations have been successful in predicting the occurrence and properties of regions of laminar attached and separated flows over adiabatic and cooled compression and expansion corners. In these analyses the common fundamental assumption is that the streamwise pressure gradient in such regions of shock wave-boundary layer interaction is generated solely by a strong interaction between the viscous and inviscid flow fields. Thus, the initial development of this viscous layer must be independent of the disturbance which promoted the interaction whether it be an incident shock or compression or expansion corner. This "free interaction" assumption has been verified experimentally for small separated regions in supersonic[16] and hypersonic flows.[17,18,19] In fact, experiment[17,18] has shown that for small separated regions, the distribution of heat transfer and pressure on the wall over the complete interaction region for wedge and externally generated shock induced interactions of equal strengths are almost identical. This result is of importance since it verifies to some extent the assumption made in the theoretical analyses that the interaction can be treated in terms of a two-point boundary value problem. Thus, the disturbance which promoted the interaction enters the problem via the downstream condition, and a unique solution is obtained by an iterative procedure to satisfy both the upstream and downstream boundary conditions simultaneously.

Most of the analyses of shock wave-boundary layer interaction have been based on the classical assumption that the static pressure remains constant across the viscous layer. Although this assumption can be justified for thin boundary layers in supersonic flow, in the high Mach number, low Reynolds number regime where laminar flows are of practical importance large pressure differences can be developed across a thick boundary layer in the separation and reattachment regions. In these flows, as shown in the present experimental study, the length of the separation region is of the same magnitude as the boundary layer thickness, and since large wedge angles are required to promote flow separation, there is pronounced curvature of the viscous layer in the reattachment zone (see Fig. 1). Under these conditions there is a

serious question as to the validity of the assumptions made in obtaining the conventional boundary layer equations from the Navier-Stokes equations.

A pressure gradient is developed normal to the surface as a result of curvature of the streamlines in the boundary layer. This curvature can be generated by the response of the boundary layer to a longitudinal pressure gradient induced by a disturbance downstream, or from the curvature of the surface upon which the boundary layer is growing. In general, the curvature at the outer edge of the boundary layer is not the same as the wall curvature; thus, the normal pressure gradient is caused by a combination of these two effects. In these flows it is possible to calculate the effect of surface curvature on boundary layer development and separation only if a simultaneous solution is obtained to the equations including the conservation equation in a direction normal to the surface.

Similar solutions to the boundary layer equations including the normal momentum equation have been derived[20-25] for a certain class of surfaces for which the boundary layer equations reduce to a set of ordinary differential equations. The solutions indicate that increasing surface curvature delays boundary layer separation. However, in these methods there is no mechanism provided for the interaction between the viscous and inviscid flow fields, and it is this mechanism which has been used in the integral methods to describe the non-similar development leading to boundary layer separation. In the similar solution the outer edge of the boundary layer assumes the curvature of the surface and this is, of course, unrealistic for small radii of curvature.

One phenomenon which has arisen when the conventional boundary layer equations have been used to describe the viscous-inviscid interaction in high Mach number flows over highly cooled walls is the supercritical boundary layer. The concept of subcritical and supercritical boundary layers was first introduced by Crocco[2] to describe the response of the boundary layer when subjected to an adverse pressure gradient acting uniformly across the viscous layer. A subcritical flow was defined as one in which $d\delta/dp$ was positive, while this quantity was negative for a supercritical boundary layer. Thus, a subcritical boundary layer will thicken when subjected to an adverse pressure

gradient, while a supercritical layer will thin under these conditions. Physically, a subcritical boundary layer is one in which the increase in the area of the streamtube beneath the sonic line is greater than the area contraction in the supersonic portion of the layer. Therefore a subcritical boundary layer can, by interacting with the inviscid stream, develop its own positive pressure gradient, whereas no such mechanism exists if the boundary layer is supercritical. Thus, within the conventional boundary layer formulation there is no mechanism by which a supercritical boundary layer can proceed smoothly to separation, a point at which the viscous layer must be subcritical regardless of the local Mach number or degree of wall cooling.

In order to overcome this problem within the framework of conventional boundary layer theory, it has been suggested that the boundary layer undergo a rapid change or jump to bring it from a supercritical to a subcritical response ahead of separation. Grange, Klineberg, and Lees[27] have developed expressions equivalent to the normal shock relationship for the magnitude of the jump, while Holden[28] has assumed that the jump is just sufficient to bring the boundary layer to a point where it exhibits a subcritical response. Measurements in the separation region of boundary layers which theoretically should exhibit a supercritical response do not indicate that the mechanism of boundary layer separation differs significantly from that of a subcritical boundary layer. Certainly there does not exist a discrete phenomenon in the separation process to which a "shock-like" characteristic could be ascribed. We believe that the supercritical-subcritical jump should be viewed as a device which must be used because of the limitations of the integral solution to the conventional boundary layer equations, and does not represent a part of the mechanism by which separation takes place.

It is clear from the experimental studies[29] of laminar regions of shock wave-boundary layer over highly cooled compression surfaces that the boundary layers which in conventional theoretical framework are classed as "supercritical" do not exhibit a supercritical response. There is no evidence of local boundary layer thinning or an increase in the heat transfer and skin friction at the beginning of the interaction region. The measurements indicate that the boundary layer thickens upstream of separation, which implies a larger area

change of the streamtubes in the subsonic region relative to the decrease in area of the streamtubes in the supersonic region of the boundary layer. This in turn implies that a pressure gradient exists across the boundary layer. It should also be noted that in these flows the extent of the upstream influence ahead of the separation point (from skin friction measurements) is of the order of the boundary layer thickness. Thus, in these flows, the assumptions made in conventional boundary layer that the normal pressure gradient can be neglected are invalid.

In order to describe properly the viscous-inviscid interaction leading to boundary layer separation in high Mach number, low Reynolds number flow, it is necessary to include the pressure variation across the boundary layer in the formulation of the mathematical model. If the effect of surface curvature on the development and separation of a boundary layer on a curved surface is to be calculated, then the normal momentum equation must be solved simultaneously with the conservation equations in the streamwise direction. In the theoretical analysis, which is described in Section 2 of this paper, we have derived an analysis to describe the viscous-inviscid interaction for attached and separated flows over two dimensional curved compression surfaces in hypersonic flow. Here we have obtained simultaneous solutions to the integral forms of the boundary layer equations for the conservation of mass, streamwise momentum, moment of streamwise momentum, normal momentum and energy. The velocity and enthalpy profiles in the viscous layer have been represented by the Cohen and Reshotko analogs of the Falkner-Skan equations and quartic polynomials. It was found that the sub-supercritical boundary is strongly dependent on the assumptions made about $\partial p/\partial y$. Even small values of $C \left(= \frac{p_w - p_e}{p_w}\right)$ were sufficient to change the response of a boundary layer from supercritical to subcritical. Comparisons are made between theoretical solutions and experimental measurements of skin friction, pressure and heat transfer from the present and previous experimental studies.

In the experimental studies described in Section 3 of this paper we examined the effect of model curvature and free stream conditions on the occurrence and properties of separated regions over two-dimensional curved surfaces. In this work, skin friction, heat transfer and pressure measurements were

made in attached and separated regions on a series of flat plate-curved surface wedge configurations. The length and radius of curvature of the curved surface were varied, as well as the length of the flat plate and the unit Reynolds number of the free stream. The skin friction measurements were used to detect the conditions and position at which incipient separation occurs; the pressure and heat transfer distributions were examined at these conditions. Pitot and cone pressure measurements were made on the separation and reattachment regions so that an estimate of the static pressure difference across the boundary layer could be made. The incipient separation conditions were correlated with model and free stream parameters.

2. THEORETICAL ANALYSIS

2.1 THE BASIC EQUATIONS

In this formulation the integral forms of the boundary layer equations are used to describe the non-similar development of attached and separated laminar boundary layers on highly cooled curved compression surfaces in hypersonic flow. A simultaneous solution is obtained to integral forms of the equations for the conservation of mass, streamwise momentum, normal momentum, moment of streamwise momentum and energy. Unlike the usual boundary layer solutions we do not assume that the pressure is constant across the boundary layer.

The boundary layer equations for two-dimensional flow with a surface oriented coordinate system are used, as shown in Fig. 2, retaining the important higher order terms

$$\frac{\partial}{\partial x}(\rho u) + \frac{\partial}{\partial y}(\rho v) = 0$$

continuity (1)

$$\rho u \frac{\partial u}{\partial x} + \rho v \frac{\partial u}{\partial y} + K \rho u v = -\frac{\partial p}{\partial x} + \frac{\partial}{\partial y}\left(\mu \frac{\partial u}{\partial y}\right)$$

x-momentum (2)

$$\rho u \frac{\partial v}{\partial x} + \rho v \frac{\partial v}{\partial y} + K \rho u^2 = -\frac{\partial p}{\partial y}$$

y-momentum (3)

$$\rho u \frac{\partial H}{\partial x} + \rho v \frac{\partial H}{\partial y} = \frac{\partial}{\partial y}\left(\frac{\mu}{P_r}\frac{\partial H}{\partial y}\right) + \frac{\partial}{\partial y}\left[\mu\left(1 - \frac{1}{P_r}\right)\frac{\partial}{\partial y}\left(\frac{u^2}{2}\right)\right]$$

energy (4)

Here we have assumed that since most of the momentum is contained in the outer region of the viscous layer in a hypersonic highly cooled flow, we can neglect the contribution of viscous terms to the normal pressure gradient. In addition, the assumption has been made that the radius of curvature of the surface is large compared with the thickness of the boundary layer.

Integrating Equation 1 across the boundary layer and defining

$$\delta^* = \int_0^\delta \left(1 - \frac{\rho u}{\rho_e u_e}\right) dy,$$

$$\frac{v_e}{u_e} = \frac{d\delta^*}{dx} - \frac{1}{\rho_e u_e}\frac{d}{dx}(\rho_e u_e)\int_0^\delta \frac{\rho u}{\rho_e u_e}\, dy \tag{5}$$

Using the Stewartson-Illingworth ransformation

$$dX = \frac{\rho_e a_e}{\rho_\infty a_\infty}\, dx \; ; \qquad dY = \frac{a_e \rho}{a_\infty \rho_\infty}\, dy$$

and

$$U = \frac{\partial \psi}{\partial Y} \; ; \qquad V = -\frac{\partial \psi}{\partial X}$$

and assuming the isentropic relationships for the flow at the outer edge of the viscous layer, Equation 5 becomes

$$\frac{(1+m_e)}{m_e(1+m_\infty)}\frac{\tan\theta}{\delta_i^*} = \frac{d}{dX}\log_e \delta_i^* \left[H - \frac{P_1}{m_e} + \frac{(1+m_e)}{m_e}(1 + S_w t)\right]$$

$$+ \frac{dH}{dX} - \frac{1}{m_e}\frac{dP_1}{dX} + \frac{d}{dX}(\log_e M_e)\left[2H - \left(\frac{\gamma+1}{\gamma-1}\right)\frac{P_1}{(1+m_e)} + \frac{3\gamma-1}{\gamma-1}\right.$$

$$\left. + \left(\frac{\gamma+1}{\gamma-1}\right)\frac{m_e}{1+m_e}H + \left(\frac{3\gamma-1}{\gamma-1}\right)S_w t + \frac{M_e^2 - 1}{m_e(1+m_e)}W\right] + \frac{(1+m_e)}{m_e}S_w \frac{dt}{dX} \tag{6}$$

where

$$H = \frac{1}{\delta_i^*}\int_0^{\delta_i}\left(1-\frac{U}{U_e}\right)\frac{U}{U_e}\,dY \quad ; \qquad P_1 = \frac{1}{\delta_i^*}\int_0^{\delta_i}\left(1-\frac{p_e}{p}\right)\frac{h}{h_e}\,dY$$

$$t = \frac{1}{\delta_i^*}\int_0^{\delta_i}\frac{S}{S_w}\,dY \quad \text{and} \quad W = \frac{1}{\delta_i^*}\int_0^{\delta_i}\frac{U}{U_e}\,dY\ .$$

Transforming Equation 2 and integrating across the boundary layer, we obtain

$$\left[H-\frac{P_1}{\gamma M_e^2}\right]\frac{d}{dX}\left(\log_e \delta_i^*\right)+\frac{dH}{dX}+\left\{\left[2H+1+S_w t\right]-\left[\frac{\gamma+1}{2\gamma}\right]\frac{P_1}{1+m_e}\right\}\frac{d}{dX}\log_e M_e$$

$$-\left(\frac{1}{\gamma M_e^2}\right)\frac{dP_1}{dX} = \frac{\nu_\infty}{a_\infty M_e(\delta_i^*)^2}\left(\frac{\rho_w\mu_w}{\rho_e\mu_e}\right)\delta_i^*\left(\frac{\partial f'}{\partial Y}\right)_w \qquad (7)$$

Transforming Equation 2, multiplying through by U, then integrating across the boundary layer, we obtain

$$\left[J-\frac{2}{\gamma M_e^2}\left(P_2+P_4-P_{13}\right)\right]\frac{d}{dX}\left(\log_e \delta_i^*\right)+\left\{\frac{dJ}{da}-\frac{2}{\gamma M_e^2}\left[\frac{\partial P_2}{\partial a}-P_{3A}+P_{6A}\right.\right.$$

$$\left.\left.-\frac{1}{P_e}\frac{dP_e}{da}\left(P_4-P_{13}\right)\right]\right\}\frac{da}{dX}+\left\{\left[3J+2S_w T\right]-\left(\frac{\gamma+1}{\gamma}\right)\frac{\left(P_2+P_3\right)}{(1+m_e)}\right.$$

$$\left.-\frac{2}{\gamma M_e^2}\left[\frac{\partial P_2}{\partial X}+P_{6M}\right]\right\}\frac{dM_e}{dX}-\frac{2}{\gamma M_e^2}\left[\frac{\partial P_2}{\partial b}+P_{6B}\right]\frac{db}{dX}-\frac{2}{\gamma M_e^2}\left[\frac{\partial P_2}{\partial c}+P_{6C}\right]\frac{dc}{dX}$$

$$=\frac{2\nu_\infty}{a_\infty M_e(\delta_i^*)^2}\delta_i^*\int_0^{\delta_i}\left(\frac{\partial U/U_e}{\partial Y}\right)^2 dY+\frac{2\nu_\infty}{a_\infty M_e(\delta_i^*)^2}\delta_i^*\int_0^{\delta_i}\left(\frac{\partial U/U_e}{\partial Y}\right)^2\left[\frac{p}{p_e}-1\right]dY \qquad (8)$$

where

$$P_2 = \frac{1}{\delta_i^*}\int_0^{\delta}\left(1-\frac{\rho_e}{\rho}\right)\frac{t}{t_e}\frac{U}{U_e}\,dY \quad ; \quad P_{3A} = \frac{1}{\delta_i^*}\int_0^{1}\left(1-\frac{\rho_e}{\rho}\right)\frac{t}{t_e}\left.\frac{\partial f'}{\partial a}\right|_\eta dY \quad ;$$

$$P_4 = \frac{1}{\delta_i^*}\int_0^{\delta_i}\left(1-\frac{\rho_e}{\rho}\right)\frac{t}{t_e}\,\eta\,\frac{\partial f'}{\partial \eta}\Big|_x\, d\eta \quad ; \quad P_5 = \frac{1}{\delta_i^*}\int_0^{1}\left(\frac{\rho}{\rho_e}-1\right)\frac{\partial f'}{\partial \eta}\Big|_x\left[\int_0^{\eta}\frac{\rho_e}{\rho}\,d\eta\right]d\eta \;;$$

$$P_6 = \frac{1}{\delta_i^*}\int_0^{1}\left(\frac{\rho}{\rho_e}-1\right)\frac{\partial f'}{\partial \eta}\Big|_x\left[\int_0^{\eta}\frac{\partial}{\partial x}\left(\frac{\rho_e}{\rho}\right)d\eta\right]d\eta \;; \quad P_{13} = \frac{1}{P_G}\int_0^{1}\left(\frac{\rho}{\rho_e}-1\right)\frac{\partial f'}{\partial \eta}\Big|_x\left[\int_0^{\eta}\eta\,\frac{\partial}{\partial \eta}\Big|_x\frac{\rho_e}{\rho}\,d\eta\right]d\eta .$$

and the definitions of the velocity, enthalpy and pressure profile parameters a , b and c are given in the Section 2.2. Integrating the normal moment equation across the boundary layer,

$$-\left[\sqrt{M_e^2-1}-\tan(\Theta-\alpha)\right]\frac{1}{(1+m_e)}\;\frac{1}{\delta_i^*}\left(\int_0^{\delta_i}\frac{U}{U_e}\,dY\right)\frac{1}{M_e}\,\frac{dM_e}{dx}\quad\frac{1}{\delta^*}\left(\frac{c}{1-}\right)\frac{1}{M_e^2-1}\left(\frac{1+m_e}{1+m_\infty}\right)^2$$

$$+\frac{1}{U_e^2\,\delta_i^*}\left(\frac{a_\infty}{a_e}\right)\frac{d}{dx}\left[U_e^2\int_0^{\delta}\frac{U}{U_e}\left(\frac{V_e}{U_e}-\frac{V}{U}\right)dY\right]+\frac{d}{dx}(\tan\alpha)\,\frac{1}{\delta_i^*}\int_0^{\delta_i}\frac{U}{U_e}\left(1-\frac{U}{U_e}\right)dY \qquad (9)$$

where

$$\int_0^{\delta}\frac{U}{U_e}\left(\frac{V_e}{U_e}-\frac{V}{U}\right)dY = \delta_i^{*2}\left(\frac{1+m_\infty}{1+m_e}\right)^{3/2}\left\{W\frac{d}{dx}\log_e\delta_i^* - W^2\frac{d}{dx}\log_e M_e\right.$$

$$-\left[\frac{d}{dx}\log_e\delta_i^* - \frac{1}{P_G}\,\frac{dP_G}{da}\,\frac{da}{dx}\right]P_4 + \left(\frac{d}{dx}\log_e M_e\right)P_8 + P_{9x}$$

$$+\left(\frac{\gamma+1}{\gamma-1}\right)\frac{m_e}{1+m_e}\left(\frac{d}{dx}\log_e M_e\right)P_{13}P_{16} + P_{16}\left[\left(\frac{d}{dx}\log_e\delta_i^* - \frac{1}{P_G}\,\frac{dP_G}{da}\,\frac{da}{dx}\right)P_{15} + \frac{dP_{15}}{dx}\right]$$

$$\left.-P_{10x} + \left(\frac{\gamma+1}{\gamma-1}\right)\frac{m_e}{1+m_e}\left(\frac{d}{dx}\log_e M_e\right)P_{11} + \left[\frac{d}{dx}\log_e\delta_i^* - \frac{1}{P_G}\,\frac{dP_G}{da}\,\frac{da}{dx}\right]P_{12}\right\}$$

where

$$P_7 = \frac{1}{P_G^2}\int_0^{1}\frac{\rho_e}{\rho}f'\left(\int_0^{\eta}\eta\,\frac{\partial f'}{\partial \eta}\,d\eta\right)d\eta \quad ; \qquad P_8 = \frac{1}{P_G^2}\int_0^{1}\frac{\rho_e}{\rho}f'\left[\int_0^{\eta}f'\,d\eta\right]d\eta \;;$$

$$P_{9x} = \frac{1}{P_G^2}\int_0^{1}\frac{\rho_e}{\rho}f'\left(\int_0^{\eta}\frac{\partial f'}{\partial x}\Big|_\eta\,d\eta\right)d\eta \quad ; \qquad P_{10x} = \frac{1}{P_G^2}\int_0^{1}\frac{\partial}{\partial x}\Big|_\eta\left(\frac{\rho_e}{\rho}\right)\left[\int_0^{\eta}f'^2\,d\eta\right]d\eta \;;$$

$$P_{11} = \frac{1}{P_G^2}\int_0^1 \frac{\rho_e}{\rho}\left[\int_0^\eta f'^2\,d\eta\right]d\eta\ ; \qquad P_{12} = \frac{1}{P_G}\int_0^1 \eta\,\frac{\partial}{\partial\eta}\Big|_x\left(\frac{\rho_e}{\rho}\right)\left[\int_0^\eta f'^2\,d\eta\right]d\eta\ ;$$

$$P_{15} = \frac{1}{P_G}\int_0^1 \frac{\rho_e}{\rho}\,d\eta\ ; \qquad P_{16} = \frac{1}{P_G}\int_0^1 (1-f')f'\,d\eta\ ; \qquad P_G = \int_0^1 (1-f')\,d\eta\ .$$

The energy equation (4), when integrated across the boundary layer, becomes

$$T\frac{d}{dX}\log_e \delta_i^* + \frac{dT}{dX} + T\frac{d}{dX}\log_e M_e = -\frac{\nu_\infty}{a_\infty M_e \delta_i^*}\frac{\delta_i^*}{S_w}\left(\frac{\partial S}{\partial Y}\right)_w\left(\frac{\rho_w \mu_w}{\rho_e \mu_e}\right) \quad (10)$$

where

$$\delta_i^* = \int_0^\delta \frac{\rho}{\rho_w}\frac{U}{U_e}\,dY$$

Equations (6), (7), (8), and (10) can be rewritten in the form

$$C_{1j}\frac{d}{dX}\log_e \delta_i^* + C_{2j}\frac{d}{dX}\log_e M_e + C_{3j}\frac{da}{dX} + C_{4j}\frac{db}{dX} + C_{5j}\frac{dc}{dX} = D_j\ .$$

Thus, we obtain a system of five simultaneous non-linear differential equations where C_{ij} and D_j are functions of the profile parameters a, b, c and M_e and δ_i^*. The term $\int_0^\delta \frac{U}{U_e}\left(\frac{V_e}{U_e} - \frac{V}{U_e}\right)dY$ contains second derivatives with respect to X. However, since its magnitude is small, it was calculated by taking the forward difference of the first derivative.

2.2 VELOCITY AND ENTHALPY PROFILES

In the earliest attempts to apply momentum integral techniques to describe the non-similar development of boundary layer in strong pressure gradients, the distributions of velocity and temperature were represented by polynomials in terms of the non-dimensionalized distance from the wall and a shape factor. Subsequently, Bray, Gadd and Woodger,[30] and Lees and Reeves[6] showed that for separated regions induced by shock wave-boundary layer interaction on an adiabatic wall, the compressible flow analogs of the Falkner-Skan profiles obtained by Cohen and Reshotko[31] better represented the form of the velocity profiles. This approach was extended successfully to flows with heat transfer by Holden,[7] and later by Klineberg and Lees,[10] by using both the velocity and enthalpy profiles from the Cohen and Reshotko solutions.

In the present analysis the Cohen and Reshotko profiles have been used to describe the distribution of velocity and enthalpy in the attached and separated viscous layer. In addition, because of the complexity of the present problem, we introduce quartic polynomials to represent the form of the velocity and total enthalpy profiles in the terms which arise when the pressure is allowed to vary across the boundary layer. The equations have been formulated in such a way that the terms in which a pressure distribution must be specified represent the difference between the analysis for $\partial p/\partial y = 0$ and $\partial p/\partial y \neq 0$. The quartic distributions for the velocity and enthalpy profiles used in these terms are matched to the Cohen and Reshotko profiles used in remaining and more important terms. The polynomial forms chosen for the velocity and enthalpy profiles were

$$\frac{U}{U_e} = \eta^2 (6 - 8\eta + 3\eta^2) + A\eta (1-\eta)^3$$

and

$$\frac{S}{S_w} = 1 - \eta^2 (6 - 8\eta + 3\eta^2) - B\eta (1-\eta)^3 \quad .$$

Here A and B are the slopes of the velocity and total enthalpy profiles at the wall, respectively. This particular representation was chosen so that $A(X)$ and $B(X)$ could be related directly to the profile parameters $a(X)$ and $b(X)$ which are used to characterize the velocity and enthalpy profiles obtained from the Cohen and Reshotko solutions. Here $a(X)$, the velocity profile parameter, is defined as $\frac{d(U/U_e)}{d(Y/\delta_i)}$ for attached flow and Y^*/δ_i for separated flow, where Y^* is the distance between the wall and the point of zone velocity in the separated shear layer. $b(X)$ is defined as the slope of the total enthalpy profile at the wall in both attached and separated flows. The Cohen and Reshotko and polynomial velocity profiles are linked by the relationship $A = a$ for attached flow, and $A = a(6 - 8a + 3a^2)/(1-a)^3$ for separated flow, (matching the point of zero velocity in the separated shear layer). For the enthalpy profiles $B = b\eta^*_{CR}$ in both attached and separated flows, where η^*_{CR} is the value of η_{CR} at $U/U_e = 0.99$. A comparison between the Cohen and Reshotko and polynomial distributions is shown in Fig. 3. Here it can be seen that the distributions are in close agreement for attached boundary layers, but show noticeable departure with significant reverse flow. It is of interest to compare

the form of the polynomial and Cohen and Reshotko velocity distributions in separated regions for identical velocity gradients at the wall, also shown in Fig. 3. The significant difference between the profiles correlated in this way is responsible in part for discrepancies between the solutions obtained from integral methods using single parameter polynomials and Cohen and Reshotko profiles.

The pressure distribution across the boundary layer is assumed to be of the form

$$\frac{p_e}{p} = 1 - c(1 - \eta^2)$$

where $c = \frac{p_w - p_e}{p}$. This form satisfies the boundary conditions at the wall and edge of the boundary layer, the momentum equation at the wall, and is in agreement with the form of the static pressure measurements of Stroud and Miller[32] across boundary layers on curved surfaces. The density distribution is calculated from the equation of state $\frac{\rho}{\rho_e} = \frac{p}{p_e}\frac{t}{t_e}$ where $\frac{t}{t_e} = (1 + S)(1 + m_e) - m_e f'^2$.

Because of the algebraic complexity of evaluating many of the integrals associated with the normal pressure gradient, both the manipulation and exact integration were performed on a digital computer using Formax. These integrals were expressed exactly in terms of A, B, C, m_e and S_w.

The integral quantities H, J, P, R, etc., which were determined from the Cohen and Reshotko solutions were fitted as a power series in a by the method of least squares and expressed in the form

$$H = c_0 + c_1 a + c_2 a^2 \ldots c_n a^n .$$

Similarly, the integrals which depended on the enthalpy profiles were fitted as a power series in b. Functions of both a and b were written in terms of component expressions composed of power series in a and b.

2.3 SOLUTION OF THE DIFFERENTIAL EQUATIONS AND COMPARISON WITH EXPERIMENT

The equations for the continuity of mass, x - momentum, moment of x - momentum, y - momentum and energy (Equations 6, 7, 8, 9 and 10) can be written as a system of five simultaneous, non-linear, ordinary differential equations of the form

$$c_{1j} \frac{d}{dX} \log_e \delta_i^* + c_{2j} \frac{d}{dX} \log_e M_e + c_{3j} \frac{da}{dX} + c_{4j} \frac{db}{dX} + c_{5j} \frac{dc}{dX} = D_j$$

where the displacement thickness δ_i^*, the local Mach number M_e and the velocity, enthalpy and pressure profile parameters a, b and c are the independent variables for which a solution must be obtained at each X station. The algebraic expressions for c_{1j}, c_{2j}, etc., are contained in Appendix 1.

These equations were solved within the framework of a two-point boundary value problem (as discussed in the Introduction) where certain of the boundary conditions upstream and downstream of the corner interaction are known. A unique solution is obtained by iterating a trial integration until all the boundary conditions, both upstream and downstream of the interaction region, are satisfied simultaneously. The integration was performed on an IBM 360 computer using a modification of the 5th order Runge-Kutta-Merson method developed at CAL by Partee.[33] A complete integration from the upstream to the downstream conditions took less than one minute, with a typical unique solution requiring approximately 15 iterations.

The integration is initialized just upstream of the corner interaction region. Here we assume the development of the velocity and enthalpy profiles to be self-similar, hence $\frac{da}{dX} = \frac{db}{dX} = 0$. If the beginning of the interaction occurs over the flat plate and the interaction between the viscous and inviscid flow in this region is "weak" ($\bar{\chi}_L$ small), then $\frac{dM_e}{dX} = 0$. Under this condition, a solution for the initial conditions yields the Blasius solution for the velocity and enthalpy distribution in the boundary layer. If the interaction over the flat plate is "strong" or the boundary layer is subjected to a pressure

gradient other than that associated with the corner interaction, then for $\frac{p}{p_\infty} \propto x^n$,

$$\left(\frac{2}{\bar{m}+1}\right) \frac{X}{M_e} \frac{dM_e}{dX} = \frac{1-\gamma}{\gamma} \left(\frac{n}{n+1}\right)$$

where $U_e = \bar{C} X^{\bar{m}}$. Hence the velocity and enthalpy profiles at the beginning of the interaction can be related to one of the family of self-similar profiles obtained from the Cohen and Reshotko solutions.

In order to proceed with a continuous integration toward the separation point, the initial response of the boundary must be such that $\frac{da}{dX}$, $\frac{db}{dX}$ and $\frac{dM_e}{dX}$ be negative while $\frac{d\delta_i^*}{dX}$ and $\frac{dc}{dX}$ are positive, i.e., the boundary layer responds in a subcritical manner. The subject of subcritical and supercritical boundary layers has been discussed at some length in the Introduction. We noted the classification was originally derived from analyses in which the classical assumption that $\partial p/\partial y = 0$ was made, and suggested that in high Mach number, low Reynolds number flows over highly cooled walls a pressure gradient generated across the boundary layer plays an important role in the mechanism of flow separation. In the present analysis we can not only calculate the pressure difference developed across the boundary layer, but also investigate the effect of a non-zero pressure gradient across the boundary layer on its initial response. We have made calculations of the effect of small positive values of c on the supercritical-subcritical boundary and found that it is extremely sensitive to this parameter. For one of the examples studied in earlier work (Ref. 29), the separation of a laminar boundary layer in Mach 20 airflow in the strong interaction regime, a value of c of just less than 0.04 changed the response of the boundary from supercritical to subcritical. We propose that, rather than using a jump condition to overcome the problems associated with the occurrence of a supercritical boundary layer, a more satisfactory approach from both the physical and mathematical viewpoints is to specify a pressure difference across the boundary layer of just sufficient magnitude to evoke a subcritical response. Since the initial value for c is far smaller than those subsequently calculated through the interaction region, its only effect is to perturb the boundary layer, causing the subsequent

subcritical development. At the downstream end of the interaction, we require both a and b to approach the Blasius profiles as the Mach number approaches the prescribed value on the wedge.

A typical solution for the basic variables a, b, c and M_e is shown in Fig. 4. Here the calculations were performed for comparison with pressure and heat transfer measurements made in a Mach 10 airflow over a highly cooled flat plate-wedge configuration, shown in Fig. 5. The pressure, heat transfer and skin friction are related to the basic variables by the relationships

$$\frac{p_w}{p_o} = \left[\frac{1+m_o}{1+m_e}\right]^{\frac{\gamma}{\gamma-1}} \frac{1}{1-c}$$

$$\frac{q}{q_o} = \left[\frac{1+m_o}{1+m_e}\right]^{\frac{3\gamma-1}{2(\gamma-1)}} \left[\frac{Q_{cR}}{Q_{cR_o}}\right] \frac{1}{\delta_R}\left(\frac{1}{1-c}\right)$$

$$\frac{c_f}{c_{f_o}} = \left[\frac{1+m_o}{1+m_e}\right]^{\frac{2\gamma-1}{\gamma-1}} \left(\frac{M_e}{M_o}\right)\left[\frac{P_{cR}}{P_{cR_o}}\right] \frac{1}{\delta_R}\left(\frac{1}{1-c}\right) .$$

At the beginning of the interaction the Mach number is less than the free stream value because of the weak interaction at the leading edge, and consequently the pressure p_o at this point is slightly larger than the static pressure of the free stream. The Mach number falls rapidly with the gradient reaching a maximum at separation, which is reflected in an inflexion in the pressure distribution at this point. Both a and b, and hence c_f and q, decrease monatonically as separation occurs, with a and, of course, c_f, equal to zero at separation. In the separated region, a (now re-defined as Y^*/δ_i^*) increases to a maximum at the point of maximum displacement, the point where b and the heat transfer rate reach a minimum. In this region the Mach number approaches a constant value, causing a region of approximately constant pressure -- the plateau pressure region. Downstream of the plateau

region the Mach number decreases through the reattachment compression process to approach asymptotically the wedge Mach number. a returns to zero at the reattachment point, and then in the attached flow downstream a and b increase to approach their Blasius values on the wedge. We note that reattachment occurs approximately halfway up the reattachment compression rise and the heat transfer is a maximum at the end of the compression process. At the beginning of the interaction we assume that c is zero or very small. c increases through the separation process, reaching a local maximum at the point of boundary layer separation. From Fig. 5 it can be seen that the effect of including the normal pressure gradient is to accentuate the pressure gradient in the separation region. Because c, and hence the pressure difference across the boundary layer, drops rapidly in the separated region, the new theory gives a more well-defined plateau pressure region than the theory with $\partial p/\partial y = 0$. Downstream of the maximum displacement thickness c increases to reach a local maximum at the reattachment point. Again the reattachment compression rise is steeper for the theory including $\partial p/\partial y$. c approaches zero as the curvature of the shear layer decreases. The present theory predicts slightly larger heat transfer rates in the separated region than the measurements or the theory with $\partial p/\partial y = 0$ indicate; however, it is in better agreement with the measurements downstream of reattachment than the more simple theory.

In the above comparison we have seen that the effect of including the normal pressure gradient in the theory is to steepen the gradient in the separation and reattachment regions, giving a better defined plateau region. However, since the boundary layer was comparatively thin, the maximum pressure ratio across the boundary was less than 1.25. In the experimental study presented in this paper, the boundary layers were an order of magnitude thicker, the Mach number was a factor of 1.5 larger, and as a consequence, the pressure rise required to separate the boundary layer and the associated turning angles of the viscous layer were significantly increased. Earlier,[29] when we attempted to make a comparison between similar experimental measurements and the theory without allowing for a normal pressure gradient, we found we were unable to integrate completely to the end of the interaction

region and thus obtain a unique solution. This problem was associated with the derivatives becoming discontinuous just downstream of reattachment, and at this time it was suggested that a possible cause of this was the failure to describe the flow accurately by allowing for normal pressure gradients. This was a stimulus toward developing the theory with $\partial p/\partial y \neq 0$. Using the present analysis, we were able to obtain complete solutions where the earlier theory had failed. A comparison between the theory and the measurements of skin friction, pressure and heat transfer made on the flat plate - 18° wedge in a Mach 14.5 airflow is shown in Fig. 6. The calculated distribution of the static pressure ratio, shown in Fig. 6a, indicates that, as observed earlier, this ratio is greatest at the separation and reattachment points; however, in this case, pressure ratios greater than 1.6 were generated across the boundary layer. Since the length of the separated region is comparatively small, a pressure gradient still exists across the viscous layer at the point of maximum displacement thickness. The predicted skin friction distribution is in agreement with the measurements, though the theory underestimates the length of the separated region. The maximum negative value occurs on the wedge as the experiments indicate, and the predicted maximum occurs at the end of the reattachment compression process and is in close agreement with the measurements. The comparison between the measured pressure distribution and the predictions for the pressure at the edge of the boundary layer and on the wall, given in Fig. 6b, show clearly the importance of the variation in pressure across the boundary layer in the analysis. Only by including the pressure rise across the boundary layer can the measured pressure rise in the separation and reattachment regions be predicted. As we observed in the comparison with the Mach 10 data, the theory overestimates the heat transfer rates in the separated region (see Fig. 6c); however, the level of heating in the reattachment region is predicted to good accuracy.

3. EXPERIMENTAL STUDIES

3.1 INTRODUCTION

In the experimental study, we examined the effect of surface curvature and Reynolds number on the occurrence and properties of separated laminar boundary layers on highly cooled compression surfaces in hypersonic airflow. Here, in addition to detecting the conditions required to promote incipient separation, by examining the position of the point of zero skin friction and the distribution of pressure and heat transfer we hoped to obtain a better understanding of the mechanism of separation on curved compression surfaces. Earlier studies by Chapman, Kuehn and Larson,[16] Kuehn,[34] and Sterrett and Emery[35] in supersonic flow had shown that the pressure rise required to promote incipient separation increases markedly when a curved surface is introduced to replace the abrupt junction of a flat plate-wedge compression surface. These measurements, which were made in both laminar and turbulent boundary layers over adiabatic surfaces, indicated that the surface curvature can increase the pressure rise to promote incipient separation by as much as a factor of 3.5.

Analytical studies[26] of the effect of surface curvature on boundary layer separation have indicated that concave curvature tends to inhibit flow separation whereas convex curvature produces the opposite effect. An important parameter controlling the magnitude of this effect was found to be the inverse root of the Reynolds number based on the local radius of curvature. These analyses are restricted to a class of similar surfaces for which the second-order boundary layer equations reduce to a set of ordinary differential equations for which similar solutions exist. In addition, it is assumed that $\delta/R \ll 1$ and there is no interaction between the viscous and inviscid flow; thus, the edge of the boundary layer follows the surface curvature and there is no mechanism for the non-similar development of the boundary layer leading to separation.

In hypersonic low Reynolds number flow, the interaction between the non-similar growth of a laminar boundary layer and the inviscid flow around a concave or convex surface is of great importance. In addition to the viscous-

inviscid interaction which would be induced in the absence of surface curvature, we have additional transverse pressure gradients generated as the boundary layer attempts to follow the curvature of the surface. The interplay between the viscous and inertial forces generated by viscous-inviscid interaction and surface curvature control the development of the viscous layer and the conditions under which separation occurs.

In the present experimental study, we attempted to explore the conditions under which the inertial forces generated by surface curvature become of importance. Beginning with a flat plate-wedge compression surface, surface curvature was introduced by interposing cylindrical sections between the flat plate and wedge. A series of circular cylindrical sections with different radii of curvature was tested; each cylindrical section contained segments which could be added or subtracted to change the degree of turning. The position and angle of the wedge was adjusted so that it formed a continuous surface tangential to the trailing edge of each cylindrical segment. In the following section, the test facilities, model geometry and instrumentation are described and the results of the studies of the flow establishment times and finite span effects are reviewed. The results from the experimental measurements are then discussed.

3.2 EXPERIMENTAL PROGRAM

This experimental program was conducted in the CAL 4-ft shock tunnel.[36] This tunnel, which operates on tailored interface principles, uses a heated helium driver. For the test conditions chosen in these studies the useful running time was approximately 5 milliseconds.

Photographs of the models are shown in Fig. 7. The models consisted of a flat plate followed by a circular cylindrical surface which terminated into a second flat plate. Cylindrical surfaces with radii of curvature of 6, 12 and 20 inches were inserted between the flat plate and ramp in the program and these surfaces were constructed in segments so that the degree of turning could be varied. The second flat plate, or ramp, was supported so that the slope at the junction between the curved surface and the ramp was continuous. The

length of the leading edge of the flat plate could be varied to give lengths of flat plate from 12 to 17 inches.

The flat plate, cylindrical sections, and ramp were fully instrumented with skin friction, heat transfer and pressure transducers (see Fig. 7). The thin film heat-transfer gages, which were coated with an insulating film of titanium dioxide, were used in conjunction with analog networks which converted their output directly into heat transfer rate. Both orifice-type and flush-mounted pressure transducers were used in the model. These exposed diaphragm-type piezoelectric transducers, described in Ref. 37, use lead zirconium titanate crystals and have a nominal sensitivity of 2 volts/psi. The skin friction transducers, described in Ref. 38, consist of a 1/4-inch diameter diaphragm mounted flush with the surface of the model, with the diaphragm connected by a fixture to a crystal mounted in bending. This transducer which is compensated for normal pressure, acceleration and thermal effects has a nominal sensitivity of 20 volts/psi.

The pitot and cone pressure probes used in the rake were 1/8-inch in diameter and had the diaphragm of the transducer mounted directly behind the orifice to ensure a maximum response. The transducer is compensated for thermal and acceleration loads and directly connected to an F.E.T. circuit to give a low output impedance. A typical sensitivity is 50 mV/psi. A double-pass schlieren system with a focal length of 10 ft was used to obtain photographs of the flow over the models.

The test program was conducted at free stream Mach numbers of 14.0 and 14.5 and Reynolds numbers of 7.2×10^4 and 1.8×10^5 per ft, respectively. Reservoir pressures of 1500 and 4200 psia were used at a common stagnation temperature of 5330°R.

3.3 TIME ESTABLISHMENT AND FINITE SPAN EFFECTS

Two important considerations in a shock tunnel study of two-dimensional compression surfaces are (a) is the flow steady? and (b) are the measurements made in a "two-dimensional flow"? Both of these questions have received

careful and extensive study during the course of the measurements in attached and separated regions on two-dimentional models. Since many of the detailed results of these studies have been published in earlier papers,[28,29] rather than present similar measurements made in the present study, we will summarize the combined conclusions.

For free stream conditions and model configurations at which the boundary layer remained completely attached, the viscous and inviscid flows were established within the starting time of the tunnel (less than 1 millisecond). The measurement indicates that it takes no longer to establish an attached boundary layer in a strong pressure gradient than it does to establish the boundary layer over a flat plate. The studies at Mach numbers from 14 to 20 and unit Reynolds numbers from 2,000/in to 14,000/in indicated that separated regions can take as long as 2.5 milliseconds to establish. Our measurements indicate that during flow establishment the leading edge of the separated region propagates forward at approximately the speed of sound of the gas close to the wall. However, we have found that in some cases boundary layers just at the incipient separation condition can take almost as long to stabilize as a large separated region.

The effect of finite model span on the properties of both attached and separated boundary layers was investigated by varying the model span and adding side fences while monitoring both the longitudinal and spanwise distributions on the model. Although increasing the model span from 1 ft to 1.5 ft did not measurably influence the properties of attached interaction regions, it did cause a small increase in the size of large separated regions. However, further increasing the span to 2 ft had little additional effect. Adding side fences to this latter configuration did influence the distribution of properties on the model. However, by adding side fences to the 1-ft span model we obtained a larger separated region than that on the 2-ft span model with or without side fences. Side fences should be used with care, for by adding them it is possible to change the basic flow. We found that a uniform distribution across the center span of the model is not a good criterion to determine whether the flow is "two-dimensional." The criterion which has been adopted here has been to

vary the transverse boundary conditions by adding spanwise extensions and side fences until successive change produced no measurable effect on the longitudinal or transverse distribution of skin friction, heat transfer or pressure on the model.

3.4 SKIN FRICTION, HEAT TRANSFER AND PRESSURE DISTRIBUTIONS

During the experimental program, skin friction, heat transfer, pressure and schlieren measurements were made on the flat plate-cylindrical surface-ramp models with radii of curvature of 0, 6, 12 and 20 inches and ramp angles from 15° to 35°. All the measurements made at a particular configuration and test condition were recorded simultaneously, and in some cases 115 data channels were required. Since insufficient space prohibits showing here all of these measurements, series of distributions are presented which are representative of the important characteristics observed in the study.

The distributions of properties typical of those found in attached and separated regions over flat plate-wedge compression surfaces are shown in Fig. 8. Here, as in earlier studies[29], the first evidence that the boundary layer was close to separation was exhibited in the character of the skin friction distribution downstream of the flat plate-wedge junction. Fig. 8a shows that the point of minimum skin friction occurs on the ramp and, as found earlier and observed in Fig. 8b, the separation bubble forms on the ramp and feeds forward as the wedge angle increases. We observe that in attached flows the influence of the wedge extends upstream less than one boundary layer thickness, and there is no evidence to support the speculation that a small separated region is always present at the flat plate-wedge junction. When separation occurs (as shown in Fig. 8b), the initial development of this region is asymmetric with the small separation bubble displaced over the ramp. The pressure and heat transfer distributions are typical of those close to incipient separation, the pressure measurements exhibiting a distinct inflexion point, while the heat transfer in the separation region is reduced significantly below the flat plate value. Increasing the wedge angle to 24° (Fig. 8c) promotes a large region of separated flow situated symmetrically about the hinge line. The pressure distribution exhibits the classical constant

pressure region, and it is interesting to note that in this region the skin friction also remains constant, indicating that the structure of the recirculation region consists of one rather than a number of counter rotating vortices. In this separated region the pressure rise to reattachment is 0.58 of the maximum pressure rise from the plateau pressure. The heat transfer reaches a maximum at the end of the reattachment compression process, and downstream of this point the surface pressure relaxes to the wedge pressure through an expansion process generated when the compression waves on the separation and reattachment regions coalesce to form the wedge shock.

Introducing circular cylindrical sections of 6-inch radius between the flat plate and wedge had only a small effect on the wedge angle to promote incipient separation and the structure of the separated regions on configurations which promoted separated flow. The distributions of surface properties for two of the configurations tested are shown in Figs. 9a and 9b. Comparing 9a with 8b, we see that for the 18° ramp angle, introducing the curved section caused a slight reduction in the length of the separated region, with the movement of the separation point on to the curved segment. The distributions to the configurations with ramp angles of 24° (shown in Fig. 9b) and 30° were practically identical to those obtained on the flat plate-wedge models with the same ramp angles (see Fig. 8c).

The first measurable effect of introducing surface curvature was evident when the flat plate-12" radius section-18° ramp was tested. The distributions shown in Fig. 10a reveal a rather important feature. The skin friction distribution shows that a small region of separated flow exists on the curved ramp. The pressure and heat transfer measurements do not give clear evidence of this. Although the pressure distribution displays some evidence of an inflexion point in the separated region, neither it nor the local heat transfer distribution could be cited to point out the existence of a separated region. Here and in the measurements of separated regions in entropy layers generated by strong bluntness, reported in Ref. 29, skin friction measurements are needed to determine accurately when separation first occurs. Adding a 6° segment to turn the flow through 24° causes a large separated region with well defined separation, plateau and reattachment regions in the pressure distribution (see Fig. 10b).

The distributions obtained over two of the configurations with the 20" radius of cylindrical section are shown in Figs. 11a and 11b. For this surface curvature the wedge angle for incipient separation has been increased to approximately 20°; however, when the wedge angle is increased, the size of the separated region increases very rapidly. The distribution for the 24° ramp angle, shown in Fig. 11a, shows the separated region, the leading edge of which has fed forward, covering the curved surface. Once the separated region moves upstream of the flat plate-curved surface junction, then the subsequent development and structure for increasing wedge angle is similar to that observed on a flat plate-wedge model (see Fig. 11b).

Finally, two of the distributions on the 12" and 20" radius compression surfaces are shown in Figs. 12a and 12b for the highest unit Reynolds number conditions. Increasing the unit Reynolds number increases the ratio of the radius of curvature to the local boundary layer thickness, which, if curvature effects are important, should cause a decrease in the length of the separated region; while we know from the measurements on flat plate-wedge surfaces that increasing the unit Reynolds number causes an increase in the size of the separated region or brings an attached region closer to separation. In each of the cases shown here, increasing the unit Reynolds number moved the separation point further forward. The curvature of the surface appeared to be of little importance once a separated region was established.

3.5 PITOT AND CONE PRESSURE MEASUREMENTS

Measurements of the pitot and cone pressure were made across the boundary layer in the separation and reattachment regions on the models in order to obtain an estimate of the pressure gradients normal to the surface in these regions. A photograph of the rake containing the conical probes is shown in Fig. 7. The probes, which are 1/8-in diameter, have the piezoelectric sensing element and the F.E.T. impedance transform circuit mounted on the cylindrical section close to the orifices. The conical tip and the pitot head are interchangeable so that the same sensing element is used to record both cone and pitot pressures. The Mach number at the tip of the probe can be

obtained from the ratio of the pitot and cone pressures; then from the Mach number and cone pressure, the local static pressure can be estimated. Although this technique is accurate at low supersonic Mach numbers, because the ratio of cone to total pressure is less sensitive to Mach number in hypersonic flow, the accuracy is estimated to be no better than 20% over the range of conditions at which our measurements were made. Fig. 13 shows schlieren photographs and the derived static pressure distributions for measurements made in the separation and reattachment regions. The measurements made just downstream of separation do not show the presence of a strong pressure gradient normal to the surface. However, the measurements in and above the reattaching boundary layer indicate that the normal pressure gradient in this region is comparable with that in the streamwise direction. Although the exact height of the boundary layer cannot be determined, using an estimate from the schlieren photographs, the total static pressure ratio across the boundary layer is found to be approximately 1.9. This figure is of the same magnitude as predicted from theory; however, it must be emphasized that the probe measurements are intended to serve only as a qualitative estimate.

3.6 INCIPIENT SEPARATION

In this study we did not find the strong dependence of incipient separation on surface curvature that was observed in the earlier studies of Kuehn,[34] and Sterrett and Emery.[35] A correlation of the incipient conditions obtained in the present study is shown in Fig. 14. Here we have plotted the product of the free stream Mach number and the angle to promote incipient separation, $M_\infty \theta_{incip}$, versus $\bar{\chi}_L^{1/2}\left(1 + \frac{Re_R}{Re_{\delta_o}}\right)$, the product of the viscous interaction parameter and the ratio of the Reynolds number based on the radius of curvature of the circular insert and the local boundary layer thickness. Earlier studies had shown that for sharp flat plate-wedge configurations $M\theta_{incip} \propto \bar{\chi}_L^{1/2}$, and for a fixed radius of curvature the configurations tested have also exhibited this trend. The ratios of radius of surface curvature to boundary layer thickness varied from 0 to 22, similar to those obtained by Kuehn, et al; however, only at the largest values of this ratio was a significant increase found in the wedge angle to promote incipient separation. It must be noted that conditions

encountered in the present study differ greatly from those obtained by Kuehn, and Sterret and Emery. Here our experiments were conducted at Mach numbers which were 2 to 5 times larger which, from the earlier studies, should amplify the curvature effect. However, the boundary layers in the present study were completely laminar as compared with the transitional or fully turbulent conditions encountered earlier, and the measurements were made on a highly cooled wall, whereas Kuehn's and Sterrett and Emery's experiments were conducted over adiabatic surfaces.

We believe that relative insensitivity of the separation condition to surface curvature results from the intrinsic structure of the laminar boundary layer on highly cooled high Mach number flows. In these flows most of the momentum contained in the boundary layer is concentrated at its outer edge; thus, in order to produce a change in its development, a slope change at the surface must be propagated almost completely across the boundary layer. If the distance travelled downstream by this disturbance ($\simeq M_e \delta$) is small compared with the projected distance along the edge of the boundary layer to the compression surface, then the initial curvature of surface is important. However, if, as in the cases studied here, the boundary layer begins to turn parallel to the curved surface only when it is in close proximity to this surface, then it is the surface curvature at this point which is of importance. The angle which the edge of the viscous layer makes with the local angle of the ramp just before appreciable turning takes place is of principal importance. If this angle is less than or equal to the wedge angle for incipient separation, $\theta_{w\,incip}$, then we would not expect separation to occur. Following this reasoning, a significant change could be expected in the incipient separation condition by introducing surface curvature only if $\frac{R\theta^2_{w\,incip}}{2} \geq \delta_L$. Since $M\theta_{w\,incip} \propto \bar{\chi}_L^{1/2}$, this criteria implies that at higher Mach numbers, for a fixed length of flat plate, an even larger radius is required before surface curvature effects are of importance.

4. CONCLUDING REMARKS

In this paper a theoretical analysis has been developed to describe the non-similar development of attached and separated laminar boundary layers in regions of shock wave-boundary layer interaction over highly cooled curved compression surfaces. No assumption was made that the pressure is constant across the boundary layer; thus, by obtaining a simultaneous solution to the integral forms of the conservation equations including the normal momentum equation, we were able to calculate the pressure difference across the boundary layer and the effect of surface curvature. The initial response of a boundary layer to a streamwise pressure gradient depends strongly on the normal pressure gradient; small values of the parameter of $\frac{p_w - p_e}{p_w}$ changed the boundary layer from supercritical to subcritical. The analysis was compared with measurements reported in this and in earlier papers and was found to be in good agreement. These calculations indicated that pressure ratios $\left(\frac{p_w}{p_e}\right)$ of the order of 1.6 are generated in the separation and reattachment regions of the flow.

In the experimental study, skin friction, heat transfer and pressure measurements were made on a series of flat plate-cylindrical arc-wedge compression surfaces to examine the effects of radius of curvature on the occurrence and structure of separated regions. Pitot and cone pressure traverses were also made to obtain an estimate of the pressure gradients normal to the surface in the separation and reattachment regions. In these flows, the first indication that flow separation was to occur was provided by the skin friction measurements on the compression surface; the skin friction was first observed to be negative on the surface downstream of the flat plate. On the compression surfaces with large radii of curvature, the incipient separation condition could not be detected with any accuracy by observing the first occurrence of an inflexion point in the pressure distribution or a change in the form of the heat transfer distribution. The static pressure distributions, evaluated from the pitot and cone pressure measurements across the boundary layers in the separation and reattachment regions, indicated that the normal pressure gradients were of the same magnitude as those in the

streamwise direction. Although the experiments were conducted for a range of ratios of δ_o/R which were similar to those used by Kuehn and Sterrett and Emery, we found that incipient separation was far less sensitive to surface curvature than indicated in these earlier studies. This we believe results from the structure of the laminar boundary layer in hypersonic flow over highly cooled walls where the streamwise distances for a surface disturbance to propagate to the edge of the boundary layer (where most of the momentum is concentrated) are greater than the length of the curved surface.

APPENDIX 1

The boundary layer equation can be written in the form

$$c_{1j}\frac{d}{dX}\log_e \delta_i^* + c_{2j}\frac{d}{dX}\log_e M_e + c_{3j}\frac{da}{dX} + c_{4j}\frac{db}{dX} + c_{5j}\frac{dc}{dX} = D_j$$

Continuity Equation ($j = 1$)

$$c_{11} = H - \frac{1}{m_e}P_1 + \left(\frac{m_e+1}{m_e}\right)(S_w t + 1)$$

$$c_{21} = 2H - \left(\frac{\gamma+1}{\gamma-1}\right)\frac{P_1}{(1+m_e)} + \left(\frac{\gamma+1}{\gamma-1}\right)\left(\frac{m_e}{1+m_e}\right)H + \left(\frac{3\gamma-1}{\gamma+1}\right)(1+S_w t) + \frac{M_e^2-1}{m_e(m_e+1)}W_{CR} - \frac{1}{m_e}\left[M_e\frac{\partial P_1}{\partial M_e}\right]$$

$$c_{31} = \frac{dH}{da} + \left(\frac{1+m_e}{m_e}\right)S_w\frac{\partial t}{\partial a} - \frac{1}{M_e}\frac{\partial P_1}{\partial A}\frac{\partial A}{\partial a}$$

$$c_{41} = \left(\frac{1+m_e}{m_e}\right)S_w\frac{\partial t}{\partial b} - \frac{1}{m_e}\frac{\partial P_1}{\partial B}\frac{dB}{db}$$

$$c_{51} = -\frac{1}{m_e}\frac{\partial P_1}{\partial c}$$

$$D_1 = \left(\frac{\nu_\infty}{a_\infty M_e \delta_i^{*2}}\right)\left(\frac{1+m_e}{m_e}\right)\frac{\tan\theta}{(1+m_e)}\left(\frac{M_e}{M_\infty}\right)Re_{\delta_{i_0}^*}\,\delta_R$$

x-Momentum Equation ($j = 2$)

$$c_{12} = H - \frac{1}{\gamma M_e^2}P_1$$

$$c_{22} = 2H + 1 + S_w t - \frac{1}{\gamma M_e^2}\left[M_e\frac{\partial P_1}{\partial M_e}\right] - \frac{(\gamma+1)}{2\gamma}\frac{P_1}{(1+m_e)}$$

$$c_{32} = \frac{dH}{da} - \frac{1}{\gamma M_e^2}\frac{\partial P_1}{\partial A}\frac{\partial A}{\partial a}$$

$$c_{42} = -\frac{1}{\gamma M_e^2}\frac{\partial P_1}{\partial B}\frac{dB}{db}$$

$$c_{52} = -\frac{1}{\gamma M_e^2}\frac{\partial P_1}{\partial c}$$

$$D_2 = \frac{\nu_\infty}{a_\infty M_e (\delta_i^*)^2}\ \frac{1}{1-c}\left[\delta_i^*\ \frac{\partial f'}{\partial Y}\right]_w$$

x-Moment of Momentum Equation ($j = 3$)

$$c_{13} = J - \frac{2}{\gamma M_e^2}\left(P_2 + P_4 - P_{13}\right)$$

$$c_{23} = 3J + 2S_w T - \left[\left(\frac{\gamma+1}{\gamma}\right)\frac{P_2}{1+m_e} + \frac{2}{\gamma M_e^2}\left(M_e\ \frac{\partial P_2}{\partial M_e}\right) + \left(\frac{\gamma+1}{\gamma}\right)\frac{P_3}{1+m_e} + \frac{2(\gamma-1)}{\gamma}\ P_{6xM}\right]$$

$$c_{33} = \frac{dJ}{dH}\ \frac{dH}{da} - \frac{2}{\gamma M_e^2}\left(\frac{dA}{da}\right)\left[\frac{\partial P_2}{\partial A} - P_{3xA} + P_{6xA} - \frac{1}{P_G}\ \frac{dP_G}{dA}\ (P_4 - P_{13})\right]$$

$$c_{43} = -\frac{2}{\gamma M_e^2}\left(\frac{\partial B}{\partial b}\right)\left[\frac{\partial P_2}{\partial B} + P_{6xB}\right]$$

$$c_{63} = -\frac{2}{\gamma M_e^2}\left[\frac{\partial P_2}{\partial c} + P_{6xC}\right]$$

$$D_3 = \frac{\nu_\infty}{a_\infty M_e \delta_i^{*2}}\left[2\,\delta_i^{*2}\int_0^\delta \left(\frac{\partial f}{\partial Y}\right)^2 dY + P_{14}\right]$$

y-Momentum Equation ($j = 4$)

$$c_{14} = 0$$

$$c_{24} = \frac{1}{(1+m_e)}\left[-\sqrt{M_e^2 - 1} + \tan(\theta - \alpha)\right] W$$

$$c_{34} = 0$$

$$c_{44} = 0$$

$$c_{54} = 0$$

$$D_4 = \frac{M_e}{M_\infty}\,\delta_{i_0}^{*}\,Re_{\delta_{i_0}^{*}}\,\delta_R^{2}\left[H\,\frac{d}{dX}\tan\alpha + \frac{c}{1-c}\;\frac{1}{\gamma M_e^{2}\delta_R\delta_{i_0}^{*}}\;\left(\frac{a_\infty}{a_e}\right)^{*}\right.$$

$$\left. + \frac{1}{M_e^{2}\delta_i^{*}}\left(\frac{a_\infty}{a_e}\right)\frac{d}{dX}\left(\delta_i^{*2}M_e^{2}\left(\frac{a_e}{a_\infty}\right)^{3}P_T\right)\right]$$

where

$$P_T = \left\{\frac{d}{dX}\log_e\delta_R\left[W_P + P_{15}\cdot P_{16} - \frac{P_{16}}{P_G} - P_7 - P_{12}\right] + \frac{d}{dX}\log_e M_e\left[-W_P^{2} + \frac{\gamma+1}{\gamma-1}\,\frac{m_e}{1+m_e}\;X\right.\right.$$

$$\left.(P_{15}P_{16} + P_{11}) + P_{10XM} + P_8\right] + \frac{d}{dX}\left[\frac{1}{P_G}\,\frac{dP_G}{dA}\,\frac{dA}{da}\left(\frac{P_{16}}{P_G} + P_7 + P_{12}\right) + P_{10XA}\,\frac{dA}{da} + P_{9XA}\,\frac{dA}{da}\right]$$

$$\left. + \frac{db}{dX}\;P_{10XB}\,\frac{dB}{db} + \frac{dc}{dX}\;P_{10XC} + P_{16}\;\frac{dP_{16}}{dX}\right\}$$

Energy Equation ($j = 5$)

$$c_{15} = T$$

$$c_{25} = T$$

$$c_{35} = \frac{\partial T}{\partial a}$$

$$c_{45} = \frac{\partial T}{\partial b}$$

$$c_{55} = 0$$

$$D_5 = -\frac{\nu_\infty}{a_\infty M_e \delta_i^{*2}}\;\left(\frac{\delta_i^{*}}{S_w}\;\frac{\partial S}{\partial Y}\right)\left(\frac{\rho_w\mu_w}{\rho_e\mu_e}\right)$$

EVALUATION OF THE INTEGRAL FUNCTIONS

Cohen and Reshotko Profiles

The integral functions H, J, W, G, P and R were evaluated from the family of velocity profiles derived by Cohen and Reshotko and expressed in the form

$$H = c_0 + c_1 a + c_2 a^2 + \cdots c_n a^n \quad .$$

Similarly, integral functions which depended only upon the enthalpy profiles were fitted as a power series in b. The functions T, t, which are functions of both a and b, we have written in the form

$$t = \frac{\int_0^{\delta_i} \frac{S}{S_w}\, dY}{\int_0^{\delta_i} \left(1 - \frac{U}{U_e}\right) dY} = \frac{I(b)}{G(a)} \quad ; \quad T = \frac{\int_0^{\delta_i} \frac{S}{S_w}\,\frac{U}{U_e}\, dY}{\int_0^{\delta_i} \left(1 - \frac{U}{U_e}\right) dY} = \frac{K(a,b)}{G(a)}$$

where K has been expressed as a function of both a and b in the form

$$K_{a=r} = c_{0r} + c_{1r} b + c_{2r} b^2 + c_{3r} b^3 .$$

The numerical values for the coefficients in these power series are presented in Ref. 28.

Polynomial Profiles

The integral functions P_1 P_2 . . . P_{15} were evaluated by exact integration of the quartic profiles where the Cohen and Reshotko and polynomial profiles are connected by the relationships.

For attached flow $A = a$ and for separated flow $A = -a[6 + a(3a - 8)] / (1 - a)^3$.

For attached flow

$$B = -12.045302 + b(177.25491 + b(-942.39173 + b(2530.4358 + b(-3382.3794 + b\,1782.0275))))$$

For separated flow

$$B = 0.024491381 + b(10.530295 + b(-27.018912 + b\,30.097469))$$

The values of P_1 . . . P_{15} are given below.

$$P_1 = \frac{1}{\rho_c}\left\{9240c - 504\,b\,S_w\,c\,(1+m_b) + 5016\,S_w\,c\,(1+m_c) + m_c\,c\,[6280 - 432a - 60a^2]\right\}/13860$$

$$P_2 = \Big\{7722ac + 4014\,(1+m_a)S_w\,ac - 637\,(1+m_c)\,b\,S_w\,ac + 16432\,(1+m_b)S_w\,c + 54912\,(1+m_b)c - 2898\,(1+m_b)\,b\,S_w c - 30480\,m_b\,c + m_b\,ac[3816 - 633a - 57a^2]\Big\}/(180180\,\rho_c)$$

$$P_{3EA} = \frac{c\,m_b}{180180}\left\{\frac{1+m_b}{m_c}[7722 + S_w(4014 - 637b)] - 1512 - 422a - 57a^2\right\}$$

$$P_4 = \frac{1}{\rho_c}\frac{c\,m_b}{360360}\left\{\frac{1+m_b}{m_c}\left[\,S_w(43368 - 1014a + b(481a - 7020)\right] + 10296\,[10 - a\,]\right] - 41136 + 564a + 254a^2 + 38a^3\right\}$$

$$P_5 = \frac{1}{\rho_c}\Big[\,ab\,S_w(1+m_c)c\left\{\frac{7c_1}{1980} + \frac{173c_2}{128700} + \frac{1849c_3}{3153150} + \frac{11651c_4}{38984400} + \frac{99409c_5}{581981400}\right\} + b\,S_w(1+m_c)\,c\left\{\frac{3c_1}{110} + \frac{79c_2}{10725} + \frac{1207c_3}{420420} + \frac{4713c_4}{5405400} + \frac{3379c_5}{44088950}\right\}$$
$$+ a\,S_w\,(1+m_b)\,c\left\{\frac{3c_1}{110} + \frac{137c_2}{11700} + \frac{1760c_3}{350350} + \frac{364733c_4}{142942800} + \frac{1267219c_5}{872872100}\right\} - S_w\,(1+m_b)\,c\left\{\frac{134c_1}{495} + \frac{2128c_2}{32175} + \frac{7850c_3}{315315} + \frac{30260c_4}{2552550} + \frac{474424c_5}{72747675}\right\}$$
$$+ a\,(1+m_b)\,c\left\{\frac{3c_1}{70} + \frac{137c_2}{7560} + \frac{113c_3}{13860} + \frac{73c_4}{17160} + \frac{223c_5}{90090}\right\} - (1+m_b)\,c\left\{\frac{38c_1}{105} + \frac{31c_2}{315} + \frac{137c_3}{3465} + \frac{14c_4}{715} + \frac{166c_5}{15015}\right\}$$
$$+ a\,m_c\,c\left\{\frac{6c_1}{1001} + \frac{23833c_2}{2627488} + \frac{163997c_3}{40738869800} + \frac{9086339c_4}{814773796400} + \frac{6103619c_5}{509681405300}\right\} + a^2m_c\,c\left\{\frac{c_1}{45045} + \frac{601c_2}{2364200} + \frac{4733c_3}{29628144} + \frac{2302009c_4}{24443218800} + \frac{8529589c_5}{147241294200}\right\}$$
$$- a^3m_c\,c\left\{\frac{19c_1}{60060} + \frac{1007c_2}{8751600} + \frac{343c_3}{6928350} + \frac{613c_4}{24504480} + \frac{3769177c_5}{265034329560}\right\} + m_c\,c\left\{\frac{600c_1}{9009} + \frac{138041c_2}{7657650} + \frac{884611c_3}{101846745} + \frac{2115797c_4}{436486050} + \frac{218018c_5}{74514825}\right\}$$
$$+ ab\,S_w(1+m_b)\left\{\frac{c_1}{252} + \frac{421c_2}{277200} + \frac{67c_3}{100100} + \frac{619c_4}{1801800} + \frac{1007c_5}{5105100}\right\} - b\,S_w(1+m_b)\left\{\frac{5c_1}{168} + \frac{127c_2}{15400} + \frac{7c_3}{2145} + \frac{159c_4}{100100} + \frac{547c_5}{618800}\right\}$$
$$- a\,S_w(1+m_b)\left\{\frac{5c_1}{168} + \frac{1750c_2}{138600} + \frac{9923c_3}{1801800} + \frac{16779c_4}{600600} + \frac{32569c_5}{20420400}\right\} + S_w(1+m_c)\left\{\frac{2c_1}{7} + \frac{137c_2}{1925} + \frac{37c_3}{1365} + \frac{947c_4}{75075} + \frac{3046c_5}{425425}\right\}$$
$$- a\,(1+m_c)\left\{\frac{c_1}{20} + \frac{3c_2}{140} + \frac{5c_3}{504} + \frac{7c_4}{1320} + \frac{9c_5}{2860}\right\} + (1+m_c)\left\{\frac{2c_1}{5} + \frac{4c_2}{35} + \frac{c_3}{21} + \frac{4c_4}{165} + \frac{2c_5}{143}\right\} - a\,m_b\left\{\frac{76c_1}{15015} + \frac{19c_2}{225225} - \frac{2813c_3}{5105100} - \frac{48883c_4}{97587950} - \frac{c_5}{2184}\right\}$$
$$+ a^2m_b\left\{\frac{c_1}{40095} + \frac{703c_2}{1801800} + \frac{251c_3}{10128900} + \frac{66292291c_4}{488864437600} + \frac{41c_5}{491400}\right\} + a^2m_c\left\{\frac{c_1}{2860} + \frac{23c_2}{180180} + \frac{263c_3}{4764760} + \frac{5363c_4}{191711520} + \frac{1517c_5}{952333520}\right\}$$
$$- m_b\left\{\frac{304c_1}{55055} + \frac{94c_2}{33575} + \frac{618c_3}{45815} + \frac{34217c_4}{4408950} + \frac{274c_5}{565525}\right\}\Big]$$

$$P_6 = \frac{1}{M_c}\frac{dM_c}{dx}\frac{(2m_b)}{\rho_c}\Big[\,a\,S_w\left\{\frac{17c_1}{840} + \frac{173c_2}{19800} + \frac{142c_3}{32175} + \frac{251c_4}{100100} + \frac{2481c_5}{1856400}\right\} - S_w\left\{\frac{4c_1}{35} + \frac{83c_2}{1925} + \frac{4c_3}{195} + \frac{282c_4}{25025} + \frac{264c_5}{38675}\right\}$$
$$- a\left\{\frac{304c_1}{60060} + \frac{76c_2}{900900} - \frac{78764c_3}{142942800} - \frac{301064c_4}{740703600} - \frac{850c_5}{2034900}\right\} - \left\{\frac{304c_1}{5005} + \frac{94c_2}{3575} + \frac{618c_3}{45815} + \frac{34217c_4}{4408950} + \frac{274c_5}{56525}\right\} + (1+S_w)\left\{\frac{2c_1}{5} + \frac{4c_2}{35} + \frac{1c_3}{21} + \frac{4c_4}{165} + \frac{2c_5}{143}\right\}$$
$$- (1+S_w)c\left\{\frac{38c_1}{105} + \frac{31c_2}{315} + \frac{137c_3}{3465} + \frac{14c_4}{715} + \frac{166c_5}{15015}\right\} + a\,(1+S_w)c\left\{\frac{3c_1}{70} + \frac{137c_2}{7560} + \frac{113c_3}{13860} + \frac{73c_4}{17160} + \frac{223c_5}{90090}\right\}$$
$$+ a^2\left\{\frac{2c_1}{8190} + \frac{703c_2}{1801800} + \frac{11044c_3}{47647600} + \frac{6629291c_4}{488864437600} + \frac{13243c_5}{158727200}\right\} + a^2\left\{\frac{1c_1}{2860} + \frac{23c_2}{180180} + \frac{263c_3}{4764760} + \frac{5363c_4}{191711520} + \frac{1517c_5}{95233520}\right\}$$
$$- b\,S_w\left\{\frac{5c_1}{168} + \frac{127c_2}{15400} + \frac{7c_3}{2145} + \frac{159c_4}{100100} + \frac{547c_5}{618800}\right\} + a\,b\,S_w\left\{\frac{c_1}{252} + \frac{421c_2}{277200} + \frac{67c_3}{100100} + \frac{619c_4}{1801800} + \frac{1007c_5}{5105100}\right\}$$
$$- a^2c\left\{\frac{19c_1}{60060} + \frac{1007c_2}{8751600} + \frac{343c_3}{6928350} + \frac{613c_4}{24504480} + \frac{3769177c_5}{265034329560}\right\} + a^2c\left\{\frac{4c_1}{180180} - \frac{1202c_2}{4712400} - \frac{260315c_3}{16295479920} - \frac{2302009c_4}{24443218800} - \frac{8529589c_5}{147241294200}\right\}$$
$$- a\,b\,S_w\,c\left\{\frac{7c_1}{1980} + \frac{173c_2}{128700} + \frac{1849c_3}{3153150} + \frac{11651c_4}{38984400} + \frac{99409c_5}{581981400}\right\} + a\,c\left\{\frac{6c_1}{1001} + \frac{166831c_2}{183783600} + \frac{163997c_3}{40738869800} - \frac{9086339c_4}{814773796400} - \frac{6103619c_5}{509681405300}\right\}$$
$$- a\,S_w\,c\left\{\frac{6c_1}{385} + \frac{3151c_2}{491400} + \frac{19573c_3}{6306300} + \frac{81119c_4}{47647600} + \frac{81241c_5}{79361100}\right\} - a\,(1+S_w)\left\{\frac{c_1}{20} + \frac{3c_2}{140} + \frac{5c_3}{504} + \frac{7c_4}{1320} + \frac{9c_5}{2860}\right\}$$
$$+ c\left\{\frac{600c_1}{9009} + \frac{138041c_2}{7657650} + \frac{884611c_3}{101846745} + \frac{2115797c_4}{436486050} + \frac{218018c_5}{74514825}\right\} + S_w\,c\left\{\frac{316c_1}{3465} + \frac{2423c_2}{75075} + \frac{512c_3}{35035} + \frac{19711c_4}{2552550} + \frac{29986c_5}{6613425}\right\}$$
$$+ b\,S_w\,c\left\{\frac{3c_1}{110} + \frac{79c_2}{10725} + \frac{1207c_3}{420420} + \frac{4713c_4}{5405400} + \frac{3379c_5}{44088950}\right\}\Big] + \frac{1}{\rho_c}\frac{da}{dx}\,c\Big[-(1+m_b)(1+S_w)\left\{\frac{38c_1}{105} + \frac{31c_2}{315} + \frac{137c_3}{3465} + \frac{14c_4}{715} + \frac{166c_5}{15015}\right\}$$
$$+ a\,(1+m_c)(1+S_w)\left\{\frac{3c_1}{70} + \frac{137c_2}{7560} + \frac{113c_3}{13860} + \frac{73c_4}{17160} + \frac{223c_5}{90090}\right\} - a^2m_c\left\{\frac{19c_1}{60060} + \frac{1007c_2}{8751600} + \frac{343c_3}{6928350} + \frac{613c_4}{24504480} + \frac{3769177c_5}{265034329560}\right\}$$
$$+ a^2m_c\left\{\frac{c_1}{45045} - \frac{1202c_2}{4712400} - \frac{260315c_3}{16295479920} - \frac{2302009c_4}{24443218800} - \frac{8529589c_5}{147241294200}\right\} - a\,b\,S_w(1+m_b)\left\{\frac{7c_1}{1980} + \frac{173c_2}{128700} + \frac{1849c_3}{3153150} + \frac{11651c_4}{38984400} + \frac{99409c_5}{581981400}\right\}$$
$$+ a\,m_b\left\{\frac{6c_1}{1001} + \frac{166831c_2}{183783600} + \frac{163997c_3}{40738869800} - \frac{9086339c_4}{814773796400} - \frac{6103619c_5}{509681405300}\right\} - a\,S_w(1+m_c)\left\{\frac{6c_1}{385} + \frac{3151c_2}{491400} + \frac{19573c_3}{6306300} + \frac{81119c_4}{47647600} + \frac{81241c_5}{79361100}\right\}$$
$$+ m_c\left\{\frac{600c_1}{9009} + \frac{138041c_2}{7657650} + \frac{884611c_3}{101846745} + \frac{2115797c_4}{436486050} + \frac{218018c_5}{74514825}\right\} + S_w(1+m_c)\left\{\frac{316c_1}{3465} + \frac{2423c_2}{75075} + \frac{512c_3}{35035} + \frac{19711c_4}{2552550} + \frac{29986c_5}{6613425}\right\}$$
$$+ b\,S_w\,(1+m_c)\left\{\frac{3c_1}{110} + \frac{79c_2}{10725} + \frac{1207c_3}{420420} + \frac{4713c_4}{5405400} + \frac{3379c_5}{44088950}\right\}\Big] + \frac{1}{\rho_c}\frac{da}{dx}\Big[-m_b\left\{\frac{1013c_1}{60060} + \frac{51c_2}{9100} + \frac{68683c_3}{28588560} + \frac{128719c_4}{105814800} + \frac{67c_5}{96900}\right\}$$
$$- a\,m_b\left\{\frac{19c_1}{8190} + \frac{557c_2}{1801800} + \frac{1861c_3}{47647600} + \frac{282601c_4}{488864437600} + \frac{1888c_5}{158727200}\right\} + 2a^2m_c\left\{\frac{c_1}{2860} + \frac{23c_2}{180180} + \frac{263c_3}{4764760} + \frac{5363c_4}{191711520} + \frac{1517c_5}{95233520}\right\}$$
$$- 2a^2m_c\,c\left\{\frac{19c_1}{60060} + \frac{1007c_2}{8751600} + \frac{343c_3}{6928350} + \frac{613c_4}{24504480} + \frac{3769177c_5}{265034329560}\right\} + 2a\,m_c\,c\left\{\frac{215c_1}{180180} + \frac{893c_2}{4712400} + \frac{68219c_3}{16295479920} + \frac{269243c_4}{24443218800} + \frac{439458c_5}{147241294200}\right\}$$
$$+ 2m_b\,c\left\{\frac{36c_1}{5005} + \frac{4721c_2}{2042040} + \frac{5063c_3}{5222910} + \frac{15641c_4}{323323500} + \frac{183611c_5}{67418175}\right\}\Big] + \frac{1}{\rho_c}\frac{db}{dx}\Big[-S_w(1+m_c)\left\{\frac{5c_1}{168} + \frac{127c_2}{15400} + \frac{7c_3}{2145} + \frac{159c_4}{100100} + \frac{547c_5}{618800}\right\}$$
$$+ a\,S_w(1+m_b)\left\{\frac{c_1}{252} + \frac{421c_2}{277200} + \frac{67c_3}{100100} + \frac{619c_4}{1801800} + \frac{1007c_5}{5105100}\right\} - a\,S_w\,c(1+m_b)\left\{\frac{7c_1}{1980} + \frac{173c_2}{128700} + \frac{1849c_3}{3153150} + \frac{11651c_4}{38984400} + \frac{99409c_5}{581981400}\right\}$$
$$+ c\,S_w(1+m_b)\left\{\frac{3c_1}{110} + \frac{79c_2}{10725} + \frac{1207c_3}{420420} + \frac{4713c_4}{5405400} + \frac{3379c_5}{44088950}\right\}\Big]$$

$$
\begin{aligned}
P_7 = \frac{1}{P_G^2}\Big[& m_e\left\{\frac{441641c - 1264431}{8817000}\right\} + b S_w a(1+m_e)\left\{\frac{664c - 503}{3603600}\right\} - S_w a(1+m_e)\left\{\frac{1118c - 1001}{900900}\right\} + a(1+m_e)\left\{\frac{57c - 407}{34650}\right\} \\
& + b S_w(1+m_e)\left\{\frac{607c - 1020}{360360}\right\} - S_w(1+m_e)\left\{\frac{10660c - 15342}{900900}\right\} - (1+m_e)\left\{\frac{2417c - 3073}{34650}\right\} + b S_w a^2(1+m_e)\left\{\frac{41c - 36}{3603600}\right\} \\
& - S_w a^2(1+m_e)\left\{\frac{406c - 470}{2802800}\right\} - a^2(1+m_e)\left\{\frac{16c + 33}{554400}\right\} - a m_e\left\{\frac{14330c - 1505563}{193993800}\right\} + a^2 m_e\left\{\frac{241176c - 80025}{1551950400}\right\} + a^3 m_e\left\{\frac{48320c - 44175}{23279256000}\right\} + a^4 m_e\left\{\frac{6579c - 6503}{4655851200}\right\}\Big]
\end{aligned}
$$

$$
\begin{aligned}
P_8 = \frac{1}{P_G^2}\Big[& m_e\left\{\frac{274822c - 807807}{5705700}\right\} + b S_w a(1+m_e)\left\{\frac{2446c - 3307}{3603600}\right\} - S_w a(1+m_e)\left\{\frac{6640c - 8748}{1801800}\right\} + a(1+m_e)\left\{\frac{1019c - 2079}{69300}\right\} \\
& + b S_w(1+m_e)\left\{\frac{6281c - 9644}{3603600}\right\} - S_w(1+m_e)\left\{\frac{2423c - 3624}{277200}\right\} - (1+m_e)\left\{\frac{623c - 1782}{9900}\right\} + b S_w a^2(1+m_e)\left\{\frac{274c - 325}{3603600}\right\} \\
& - S_w a^2(1+m_e)\left\{\frac{1142c - 1325}{2402400}\right\} - a^2(1+m_e)\left\{\frac{544c - 603}{554400}\right\} + a m_e\left\{\frac{2211120c - 5007573}{193993800}\right\} + a^2 m_e\left\{\frac{1901304c - 2740655}{1551950400}\right\} \\
& + a^3 m_e\left\{\frac{267091c - 334305}{23279256000}\right\} + a^4 m_e\left\{\frac{30601c - 35207}{4655851200}\right\}\Big]
\end{aligned}
$$

$$
\begin{aligned}
P_9 = \frac{1}{P_G^2}\frac{da}{dX}\Big[& b S_w a(1+m_e)\left\{\frac{274c - 325}{3603600}\right\} - S_w a(1+m_e)\left\{\frac{1142c - 1325}{2402400}\right\} - a(1+m_e)\left\{\frac{544c - 603}{554400}\right\} + b S_w(1+m_e)\left\{\frac{1823c - 2517}{3603600}\right\} \\
& - S_w(1+m_e)\left\{\frac{9777c - 13126}{3603600}\right\} - (1+m_e)\left\{\frac{151c - 329}{12600}\right\} + a m_e\left\{\frac{1461224c - 2152491}{1551950400}\right\} + m_e\left\{\frac{2078223c - 7827373}{387987600}\right\} \\
& + a^2 m_e\left\{\frac{70085c - 98071}{775975200}\right\} + a^3 m_e\left\{\frac{30601c - 35207}{4655851200}\right\}\Big]
\end{aligned}
$$

$$
\begin{aligned}
P_{10} = \frac{1}{m_e}\frac{dm_e}{dX}\frac{(2m_e)}{P_G^2}\Big[& \frac{113}{7350} + \frac{51S_w}{5775} - \frac{251bS_w a}{400400} - \frac{1637bS_w}{900900} - \frac{bS_w a^2}{9240} - \frac{619c(1+S_w)}{13860} - \frac{29ca(1+S_w)}{2772} - \frac{ca^2(1+S_w)}{660} - \frac{2355630a^2}{857656800} - \frac{6350a^3}{305841600} - \frac{a^4}{127008} \\
& - \frac{1605118a}{71471400} + \frac{5777cbS_w a}{12612600} + \frac{29483cbS_w}{25225200} + \frac{cbS_w a^2}{11760} + \frac{6437180c}{185175900} + \frac{100787cS_w a}{12612600} + \frac{100827cS_w}{2802800} + \frac{1025cS_w a^2}{1009008} + \frac{50357380ca}{6110804700} + \frac{51360161ca^2}{36664828200} \\
& + \frac{5065133ca^3}{48886437600} + \frac{61ca^4}{9200376} + \frac{a(1+S_w)}{45} + \frac{a^2(1+S_w)}{360} - \frac{17057S_w a}{900900} - \frac{779S_w a^2}{360360}\Big] + \frac{1}{P_G^2}\frac{da}{dX}\Big[-\frac{1600018am_e}{1715313600} - \frac{15798a^2m_e}{79168[illegible]} - \frac{a^3m_e}{65[illegible]} - \frac{65953m_e}{23823[illegible]} - \frac{761163cm_e}{452552200} \\
& + \frac{2790582cam_e}{4073[illegible]} + \frac{7361126ca^2m_e}{48886437600} + \frac{122ca^3m_e}{9200376}\Big] + \frac{1}{P_G^2}\frac{db}{dX}\Big[-\frac{251aS_w(1+m_e)}{400400} - \frac{1637S_w(1+m_e)}{900900} - \frac{S_w a^2(1+m_e)}{9240} + \frac{5777cS_w a(1+m_e)}{12612600} \\
& + \frac{29483cS_w(1+m_e)}{25225200} + \frac{cS_w a^2(1+m_e)}{11760}\Big] + \frac{1}{P_G^2}\frac{dc}{dX}\Big[-\frac{619(1+m_e)(1+S_w)}{13860} - \frac{29a(1+m_e)(1+S_w)}{2772} - \frac{a^2(1+m_e)(1+S_w)}{660} \\
& + \frac{5777bS_w a(1+m_e)}{12612600} + \frac{29483bS_w(1+m_e)}{25225200} + \frac{bS_w a^2(1+m_e)}{11760} + \frac{6437180m_e}{185175900} + \frac{100787S_w a(1+m_e)}{12612600} + \frac{100827S_w(1+m_e)}{2802800} + \frac{1025S_w a^2(1+m_e)}{1009008} + \frac{50357380am_e}{6110804700} \\
& + \frac{51360161a^2m_e}{36664828200} + \frac{5065133a^3m_e}{48886437600} + \frac{61a^4m_e}{9200376}\Big]
\end{aligned}
$$

$$
\begin{aligned}
P_{11} = \frac{1}{P_G^2}\Big[& -\frac{289m_e}{2450} + \frac{5777cbS_w a(1+m_e)}{12612600} - \frac{251bS_w a(1+m_e)}{400400} - \frac{2033cS_w a(1+m_e)}{1146600} + \frac{2963S_w a(1+m_e)}{900900} - \frac{29ca(1+m_e)}{2772} \\
& + \frac{a(1+m_e)}{45} + \frac{29483cbS_w(1+m_e)}{25225200} - \frac{1637bS_w(1+m_e)}{900900} - \frac{147137cS_w(1+m_e)}{25225200} + \frac{17S_w(1+m_e)}{1925} - \frac{619c(1+m_e)}{13860} + \frac{cbS_w a^2(1+m_e)}{11760} \\
& - \frac{bS_w a^2(1+m_e)}{9240} - \frac{229cS_w a^2(1+m_e)}{450640} + \frac{37S_w a^2(1+m_e)}{60060} - \frac{ca^2(1+m_e)}{660} + \frac{a^2(1+m_e)}{360} + \frac{2(1+m_e)}{15} + \frac{50357380cam_e}{6110804700} - \frac{289am_e}{14700} \\
& + \frac{6437180cm_e}{185175900} + \frac{51360161ca^2m_e}{36664828200} - \frac{323a^2m_e}{117600} + \frac{5065133ca^3m_e}{48886437600} - \frac{17a^3m_e}{105840} + \frac{61ca^4m_e}{9200376} - \frac{a^4m_e}{127008}\Big]
\end{aligned}
$$

$$
\begin{aligned}
P_{12} = \frac{1}{P_G^2}\Big[& \frac{-399101m_e}{5955950} - \frac{2923S_w}{75075} - \frac{4259cbS_w a(1+m_e)}{12612600} + \frac{10319cS_w a(1+m_e)}{6306300} + \frac{163ca(1+m_e)}{6930} - \frac{1817cbS_w(1+m_e)}{1401400} + \frac{75631cS_w(1+m_e)}{12612600} \\
& + \frac{1229c(1+m_e)}{6930} - \frac{cbS_w a^2(1+m_e)}{21560} + \frac{509cS_w a^2(1+m_e)}{2522520} + \frac{ca^2(1+m_e)}{396} - \frac{12403cbS_w am_e}{12612600} + \frac{2053bS_w am_e}{1201200} \\
& + \frac{202cS_w am_e}{35035} - \frac{1403S_w am_e}{150150} - \frac{3516361cam_e}{179729550} - \frac{100621am_e}{35735700} - \frac{24823cbS_w m_e}{6306300} + \frac{1783bS_w m_e}{225225} + \frac{1717cS_w m_e}{84084} - \frac{2923S_w m_e}{75075} - \frac{5210377cm_e}{30171825} - \frac{53cbS_w a^2m_e}{420420} \\
& + \frac{5bS_w a^2m_e}{24024} + \frac{71cS_w a^2m_e}{84084} - \frac{19S_w a^2m_e}{15015} - \frac{101907141ca^2m_e}{36664828200} + \frac{30347a^2m_e}{50450400} - \frac{12507853ca^3m_e}{48886437600} + \frac{83159a^3m_e}{257297040} - \frac{277ca^4m_e}{18960480} + \frac{473a^4m_e}{28068768} \\
& - \frac{12403cbS_w a}{12612600} + \frac{2053bS_w a}{1201200} + \frac{202cS_w a}{35035} - \frac{1403S_w a}{150150} - \frac{24823cbS_w}{6306300} + \frac{1783bS_w}{225225} + \frac{1717cS_w}{84084} - \frac{53cbS_w a^2}{420420} + \frac{5bS_w a^2}{24024} + \frac{71cS_w a^2}{84084} - \frac{19S_w a^2}{15015}\Big]
\end{aligned}
$$

$$
\begin{aligned}
P_{13} = \frac{1}{P_G}\Big[& (1+m_e)ABcS_w\Big\{c_1\Big(\frac{37}{27720} + \frac{2}{2310}\Big) + c_2\Big(\frac{499}{900900} + \frac{1258}{3603600}\Big) + c_3\Big(\frac{3659}{12612600} + \frac{1046}{6306300}\Big) + c_4\Big(\frac{2719}{16403400} + \frac{4258}{47647600}\Big) + c_5\Big(\frac{12993}{129329200} + \frac{2798}{52907400}\Big)\Big\} \\
& - (1+m_e)ABS_w\Big\{\frac{1c_1}{504} + \frac{241c_2}{277200} + \frac{277c_3}{600600} + \frac{479c_4}{1801800} + \frac{479c_5}{2917200}\Big\} - (1+m_e)BcS_w\Big\{c_1\Big(\frac{13}{4620} + \frac{23}{4620}\Big) + c_2\Big(\frac{733}{300300} + \frac{529}{300300}\Big) + c_3\Big(\frac{37}{28028} + \frac{2}{2548}\Big) \\
& + c_4\Big(\frac{2517}{3403400} + \frac{9}{22100}\Big) + c_5\Big(\frac{1117}{2519400} + \frac{638}{2713200}\Big)\Big\} + (1+m_e)BS_w\Big\{\frac{1c_1}{168} + \frac{181c_2}{46200} + \frac{3c_3}{1430} + \frac{17c_4}{14300} + \frac{447c_5}{618800}\Big\} \\
& + (1+m_e)AcS_w\Big\{c_1\Big(\frac{86}{9240} - \frac{3}{154}\Big) + c_2\Big(\frac{3142}{675675} - \frac{38}{5005}\Big) + c_3\Big(\frac{5506}{2102100} - \frac{67}{19110}\Big) + c_4\Big(\frac{6074}{4331600} - \frac{4419}{2382380}\Big) + c_5\Big(\frac{25790}{24418800} - \frac{5741}{5290740}\Big)\Big\}
\end{aligned}
$$

$$+ (1+m_e) A S_w \left\{ \frac{1c_1}{42} + \frac{331 c_2}{34650} + \frac{97 c_3}{21450} + \frac{61 c_4}{25025} + \frac{671 c_5}{464100} \right\} + (1+m_e) c S_w \left\{ c_1 \left(\frac{130}{1155} - \frac{32}{693} \right) + c_2 \left(\frac{508}{15015} - \frac{148}{6825} \right) + c_3 \left(\frac{1762}{105105} - \frac{248}{21021} \right) \right.$$

$$\left. + c_4 \left(\frac{723}{85085} - \frac{1646}{232050} \right) + c_5 \left(\frac{251}{51870} - \frac{2332}{508725} \right) \right\} - (1+m_e) S_w \left\{ \frac{1c_1}{7} + \frac{281 c_2}{5775} + \frac{46 c_3}{2145} + \frac{278 c_4}{25025} + \frac{71 c_5}{11050} \right\}$$

$$+ m_e A c \left\{ c_1 \left(\frac{41}{6006} - \frac{93}{5005} - \frac{149}{30030} + \frac{5}{546} \right) + c_2 \left(\frac{663006}{183783600} - \frac{30302}{5105100} - \frac{5006}{2552550} + \frac{1018}{765400} \right) + c_3 \left(\frac{17191274}{8147730600} - \frac{210842}{56581525} - \frac{503746}{543182640} \right. \right.$$

$$\left. \left. + \frac{54154}{543182640} \right) + c_4 \left(\frac{208514}{156687300} - \frac{110270}{54318264} - \frac{44578}{[illegible]} - \frac{107078}{[illegible]} \right) + c_5 \left(\frac{11332014}{[illegible]} - \frac{4100366}{[illegible]} - \frac{26302}{[illegible]} - \frac{97562}{[illegible]} \right) \right\}$$

$$+ m_e A \left\{ c_1 \left(\frac{73}{3003} - \frac{149}{20020} \right) + c_2 \left(\frac{362}{34650} - \frac{37}{300300} \right) + c_3 \left(\frac{31014}{5955950} + \frac{7246}{11438432} \right) + c_4 \left(\frac{350178}{[illegible]} + \frac{118230}{[illegible]} \right) + c_5 \left(\frac{3578}{2034900} + \frac{186}{452200} \right) \right\}$$

$$+ m_e c \left\{ c_1 \left(\frac{1538}{15015} - \frac{1472}{45045} \right) + c_2 \left(\frac{48848}{1276275} - \frac{126614}{7657650} \right) + c_3 \left(\frac{2379226}{135795660} - \frac{95806}{101846745} \right) + c_4 \left(\frac{536608}{58198140} - \frac{97822}{16787925} \right) + c_5 \left(\frac{168898}{31461815} - \frac{777296}{2022545325} \right) \right\}$$

$$- m_e \left\{ \frac{1966 c_1}{15015} + \frac{1282 c_2}{25025} + \frac{57814 c_3}{2382380} + \frac{115526 c_4}{8817900} + \frac{1318 c_5}{169575} \right\} + m_e A^2 c \left\{ c_1 \left(\frac{2}{2145} - \frac{1}{2730} - \frac{46}{51480} - \frac{2}{5005} \right) + c_2 \left(\frac{118}{294525} - \frac{142}{486200} - \frac{4462}{30630600} - \frac{222}{1701700} \right) \right.$$

$$+ c_3 \left(\frac{124606}{626749200} - \frac{161134}{1086365280} + \frac{4054}{1018467450} - \frac{14866}{271591320} \right) + c_4 \left(\frac{597994}{5431826400} - \frac{20090}{279351072} + \frac{445054}{16295479200} - \frac{634}{23279256} \right)$$

$$\left. + c_5 \left(\frac{281576}{4247345025} - \frac{538442}{11779303536} + \frac{3236638}{126206823600} - \frac{1154}{75508356} \right) \right\} + m_e A^2 \left\{ c_1 \left(\frac{83}{180180} + \frac{1}{1430} \right) + c_2 \left(\frac{1}{2310} - \frac{223}{1801800} \right) + c_3 \left(\frac{190}{879648} - \frac{40914}{285885600} \right) \right.$$

$$\left. + c_4 \left(\frac{12398}{107442720} - \frac{336758}{2506096800} \right) + c_5 \left(\frac{1418}{21162960} - \frac{30746}{317444400} \right) \right\} + m_e A^3 c \left\{ c_1 \left(\frac{1}{15015} + \frac{1}{6006} \right) + c_2 \left(\frac{257}{10210200} + \frac{998}{15315300} \right) + c_3 \left(\frac{15454}{1357956600} + \frac{174266}{5431826400} \right) \right.$$

$$\left. + c_4 \left(\frac{3214}{543182640} + \frac{22714}{1303638336} \right) + c_5 \left(\frac{1658}{485410860} + \frac{1361714}{132517164780} \right) \right\} - m_e A^3 \left\{ \frac{2 c_1}{8580} + \frac{17 c_2}{180180} + \frac{2666 c_3}{57177120} + \frac{165878 c_4}{6518191680} + \frac{718 c_5}{[illegible]} \right\} \Bigg]$$

$$P_{14} = 2P_G \left[\left(\frac{48c_1}{35} + \frac{8c_2}{35} + \frac{24c_3}{385} + \frac{16c_4}{715} + \frac{48c_5}{5005} \right) - a \left(\frac{4c_1}{35} + \frac{c_2}{15} + \frac{26c_3}{1155} + \frac{19c_4}{2145} + \frac{4c_5}{1001} \right) + a^2 \left(\frac{3c_1}{35} + \frac{2c_2}{315} + \frac{c_3}{462} + \frac{9c_4}{10010} + \frac{19c_5}{45045} \right) \right]$$

$$P_{15} = \frac{1}{P_G} \left[\left\{ (1+m_e) + (1+m_e) S_w (0.4 - 0.05B) \right\} - m_e \left\{ \frac{1836 + 153A + 15A^2}{3780} \right\} - c(1+m_e) \left\{ \frac{140 + S_w(76 - 9B)}{210} \right\} + c\, m_e \left\{ \frac{2960 + 432A + 49A^2}{13860} \right\} \right]$$

$$P_G = \frac{1}{20} (B - A)$$

where

$$c_1 = c(1 + c(1 + c(1 + c)))$$

$$c_2 = -c(1 + c(2 + c(3 + 4c)))$$

$$c_3 = c(c + c(3 + 6c))$$

$$c_4 = -c^3(1 + 4c)$$

$$c_5 = c^4$$

REFERENCES

1. Crocco, L. and Lees, L. "A Mixing Theory for the Interaction between Dissipative Flows and Nearly Isentropic Streams," J. Aero. Sci., Vol. 19, No. 10, pp. 649-676 (October 1952)

2. Crocco, L., "Considerations on the Shock-Boundary Layer Interaction," Proceedings Conference on High-Speed Aeronautics, Polytechnic Institute of Brooklyn, pp. 75-112, January 20-22, 1955

3. Glick, H. S., "Modified Crocco-Lees Mixing Theory for Supersonic Separated and Reattaching Flows," J. Aero. Sci., Vol. 29, No. 10, pp. 1238-1244 (October 1962)

4. Tani, I., "On the Approximate Solution of the Laminar Boundary Layer Equations," J. Aero. Sci., Vol. 21, No. 7, pp. 487-504 (July 1954)

5. Abbott, E. E., Holt, M., and Nielsen, J. N., "Investigation of Hypersonic Flow Separation and its Effect on Aerodynamic Control Characteristics," VIDYA Report No. 81 (September 1962)

6. Lees, L. and Reeves, B. L., "Supersonic Separated and Reattaching Laminar Flows: I. General Theory and Application to Adiabatic Boundary Layer-Shock Wave Interactions," GALCIT Tech. Report No. 3 (October 1963)

7. Holden, M. S., "An Analytical Study of Separated Flow Induced Shock Wave-Boundary Layer Interaction," CAL Report No. AI-1972-A-3 (December 1965)

8. Dorodnitsyn, A. A., "General Method of Integral Relations and its Application to Boundary Layer Theory," Advances in Aero. Sci., Vol. 3 (von Karman Ed., 1962)

9. Nielsen, J. N., Lynes, L. L., and Goodwin, F. K., "Theory of Laminar Separated Flows on Flared Surfaces Including Supersonic Flow with Heating and Cooling," AGARD Conference Proc. No. 6, Part I, Proc. of AGARD Fluid Dynamics Panel held in Rhode-Saint-Genise, Belgium, May 10-13, 1966

10. Klineberg, J. and Lees, L., "Theory of Laminar Viscous-Inviscid Interactions in Supersonic Flow," AIAA Paper No. 69-7 (January 1969)

11. Flugge-Lotz, I., "The Computation of Compressible Boundary Layer Flow," "Nonlinear Partial Differential Equations," (Academic Press 1967)

12. Reyhner, T. A. and Flugge-Lotz, I., "The Interaction of a Shock Wave with a Laminar Boundary Layer," Int. J. Non-linear Mechanics, Vol. 3, pp. 173-199 (Pergamon Press 1968)

13. Baum, E. and Denison, M. R., "Interacting Supersonic Laminar Wake Calculations by the Finite Difference Method," AIAA J. 5, pp. 1224-1230 (1967)

14. Baum, E., "An Interaction Model of a Supersonic Laminar Boundary Layer on Sharp and Rounded Backward Facing Steps," BSD-TR-67-181 (July 1967)

15. Tyson, T. J., "Laminar Boundary Layers in the Neighborhood of Abrupt Spatial Disturbances," California Institute of Technology Ph.D. Thesis (June 1967)

16. Chapman, D. R., Kuehn, D. M., and Larson, H. K., "The Investigation of Separated Flows in Supersonic and Subsonic Streams with Emphasis on the Effects of Transition," NACA Report No. 1356 (1958)

17. Holden, M. S., "Experimental Studies of Separated Flows at Hypersonic Speeds. Part II, Two-Dimensional Wedge Separated Flow Studies," AIAA J. Vol. 4, No. 5, pp. 790-799 (1966)

18. Needham, D. A., Stollery, J. L., "Hypersonic Studies of Incipient Separation and Separated Flows," AGARD Conference Proc. No. 4 (May 1966)

19. Lewis, J. E., Kubota, T., and Lees, L., "Experimental Investigation of Supersonic Laminar, Two-Dimensional Boundary Layer Separation in a Compression Corner," AIAA J., Vol. 6, No. 1, pp. 7-15 (January 1968)

20. Murphy, J. S., "Some Effects of Surface Curvature on Laminar Boundary-Layer Flow," J. Aero. Sci., Vol. 20, pp. 338-344 (1953)

21. Murphy, J. S., "Extension of the Falkner-Skan Similar Solutions of the Laminar Boundary Layer to Flows with Surface Curvature," Douglas Aircraft Company, Inc. Report ES 40487 (August 1961)

22. Yen, K. T. and Toba, K., "A Theory of Two-Dimensional Boundary Layers over a Curved Surface," J. Aero. Sci., Vol. 28, pp. 877-884 (1961)

23. Hayasi, N., "Effects of Surface Curvature on Laminar Boundary-Layer Flow," AIAA J., Vol. 1, pp. 914-915 (1963)

24. Tani, I., "Some Effects of Surface Curvature on the Velocity Distribution in a Laminar Boundary-Layer," Journal of the Japan Society of Mechanical Engineers, Vol. 52, pp. 476-477

25. Van Dyke, M., "Higher Approximations in Boundary Layer Theory , Part I - General Analysis," J.F.M. Vol. 14, Part 2, pp. 161-177 (1962); "Part II - Application to Leading Edges," J.F.M. Vol. 14, Part 4, pp. 481-495 (1962)

26. Massey, D. S. and Clayton, B. R., "Laminar Boundary Layers and Their Separation for Curved Surfaces," A.S.M.E. Journal of Basic Engineering, pp. 483-484 (June 1965)

27. Grange, J. M., Klineberg, J. M., and Lees, L., "Laminar Boundary Separation and the Near-Wake Flow for a Smooth Blunt Body at Supersonic and Hypersonic Speeds," AIAA Jou Vol. 5, No. 6, pp. 1096-1098 (June 1967)

28. Holden, M. S., "Theoretical and Experimental Studies of Laminar Flow Separation on Flat Plate-Wedge Compression Surfaces in the Hypersonic Strong Interaction Regime," CAL Report No. AF-1894-A-2 (May 1967) also ARL Report No. 67-0112

29. Holden, M. S., "Leading-Edge Bluntness and Boundary-Layer Displacement Effect on Attached and Separated Laminar Boundary Layer in a Compression Corner," AIAA 6th Aerospace Science Meeting, AIAA Paper No. 68-68 (January 1968)

30. Bray, K. N. C., Gadd, G. E., and Woodger, M., "Some Calculations by the Crocco-Lees and Other Methods of Interactions between Shock Waves and Laminar Boundary Layer, including Effects of Heat Transfer and Suction," A.R.C. Report No. C.P. 556 (1960)

31. Cohen, C. B. and Reshotko, E., "Similar Solutions for the Compressible Laminar Boundary Layer with Heat Transfer and Pressure Gradient," NACA Report No. 1293 (1956)

32. Stroud, J. F. and Miller, L. D., "Hypersonic Inlet Boundary Layer," Presented at AIAA Propulsion Conference (May 1964)

33. Partee, S., "A Modified Runge-Kutta-Merson Method," CAL Library Program Manual (February 1968)

34. Kuehn, D. M., "Experimental Investigation of the Pressure Rise Required for the Incipient Separation of Turbulent Boundary Layers in Two-Dimensional Supersonic Flow," NASA Memo No. 1-21-59A (February 1959)

35. Sterrett, J. R. and Emery, J. C., "Experimental Separation Studies of Two-Dimensional Wedges and Curved Surfaces at Mach Numbers of 4.8 to 6.2," NACA TND-1014

36. "Description and Capabilities of the CAL 48-Inch Hypersonic Shock Tunnel," Cornell Aeronautical Laboratory, Inc., Buffalo, New York (April 1968)

37. Martin, J. F., Duryea, G. R., and Stevenson, L. M., "Instrumentation for Force and Pressure Measurements in a Hypersonic Shock Tunnel," Advances in Hypervelocity Techniques, CAL Report No. 113 (Plenum Press 1962)

38. MacArthur, R. C., "Contoured Skin Friction Transducer," CAL Report No. AN-2403-Y-I (August 1967)

39. Cheng, H.K., Hall, J.G., Golian, T.C., and Hertzberg, A., "Boundary Layer Displacement and Leading-Edge Bluntness Effects in High-Temperature Hypersonic Flow". J.Aero/Space Sci. Vol. 28, No. 5, pp. 353-381 (1961)

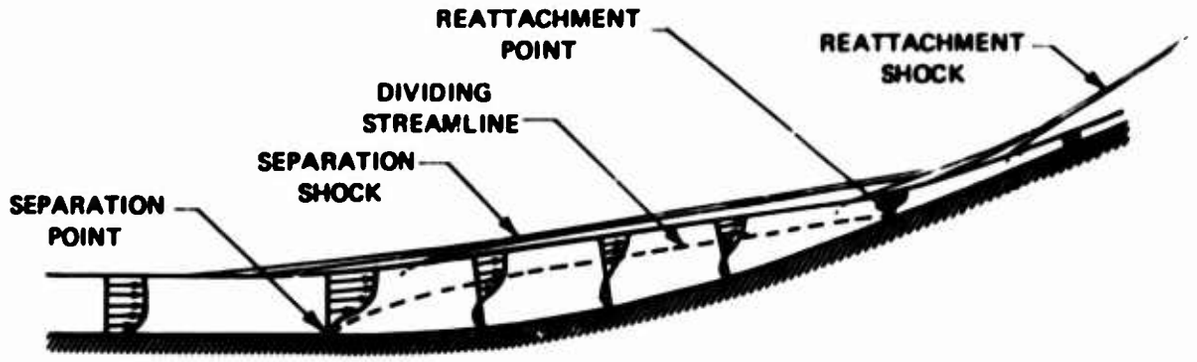

Figure 1 LAMINAR SEPARATED FLOW OVER A CURVED COMPRESSION SURFACE

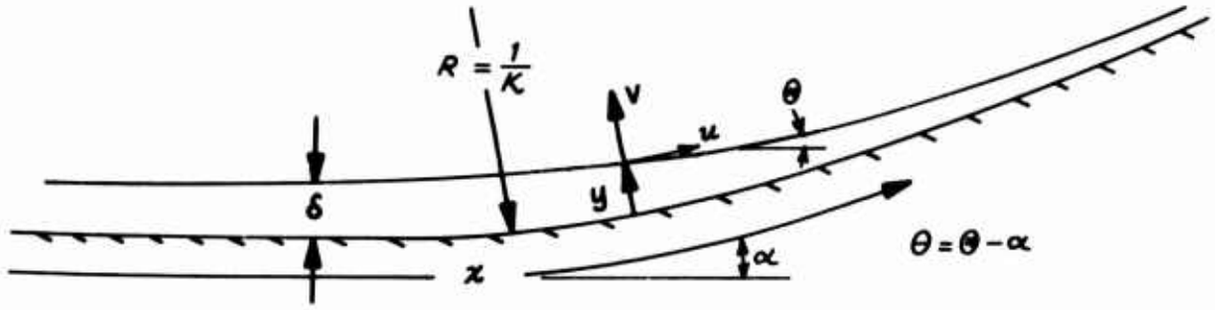

Figure 2 THE BODY ORIENTED COORDINATE SYSTEM

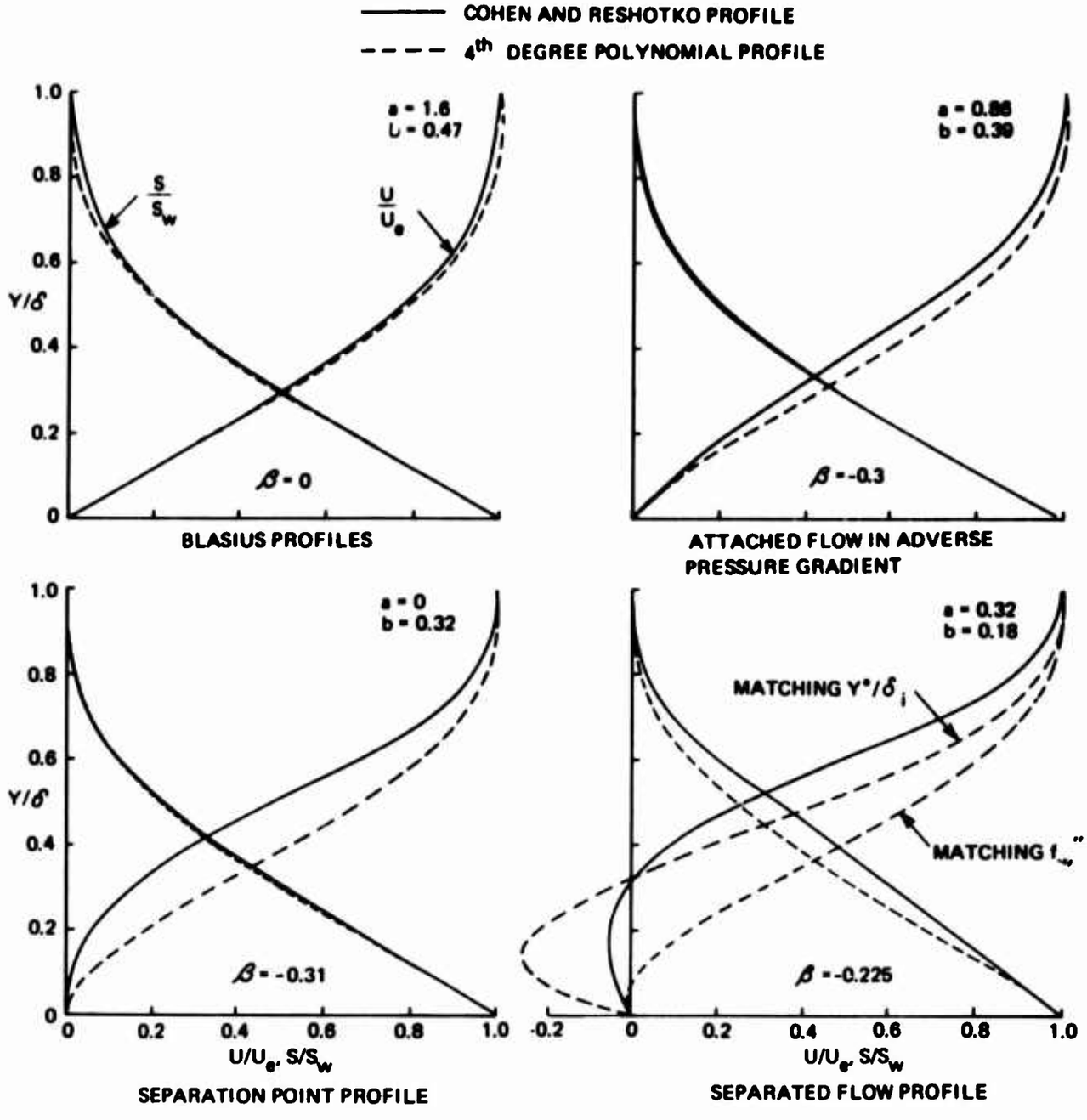

Figure 3 A COMPARISON BETWEEN COHEN AND RESHOTKO AND POLYNOMINAL PROFILES

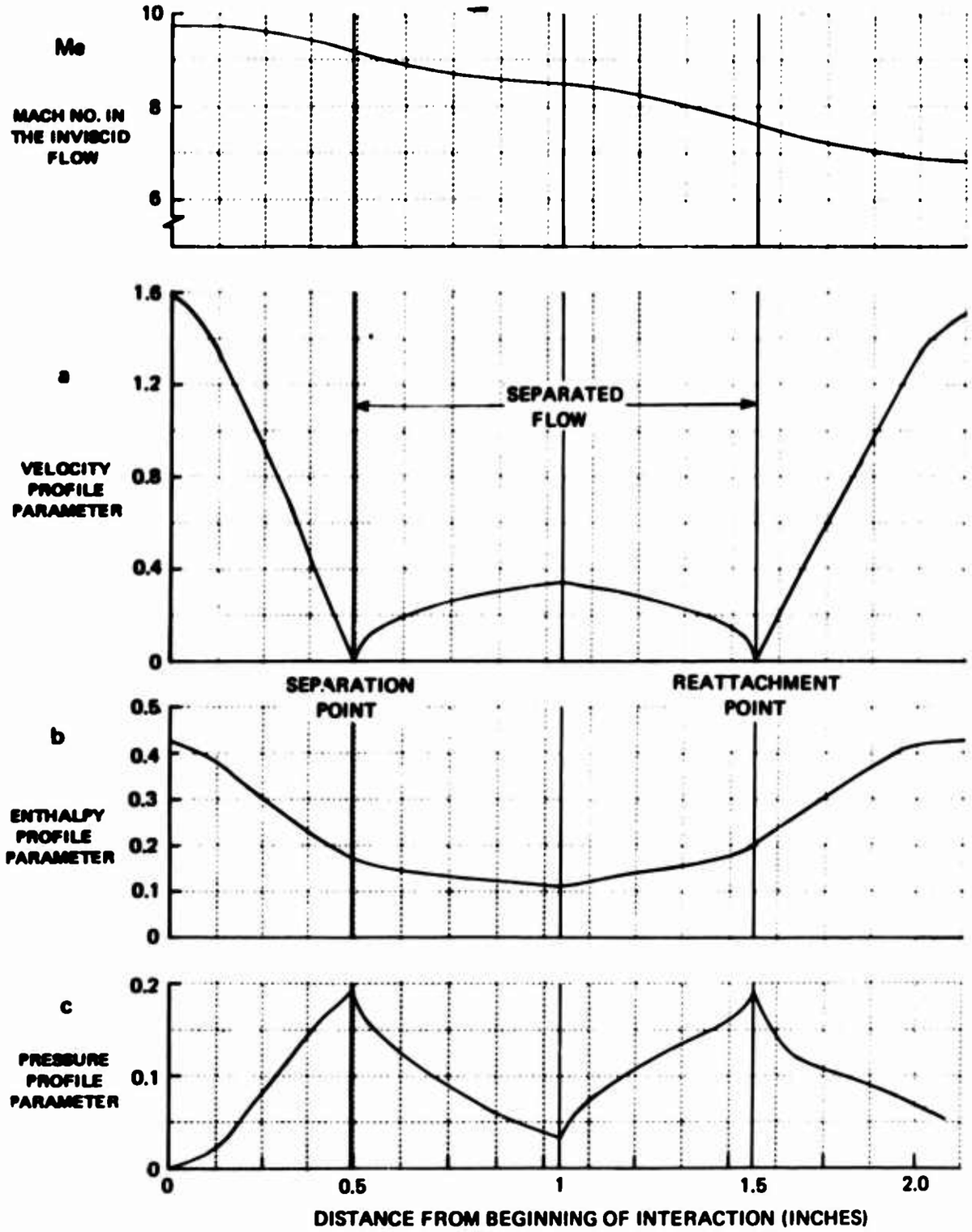

Figure 4 DISTRIBUTION OF PROFILE PARAMETERS
(M_∞ = 10, Re_L = 8.1 x 10^5, θ_w = 12.5°)

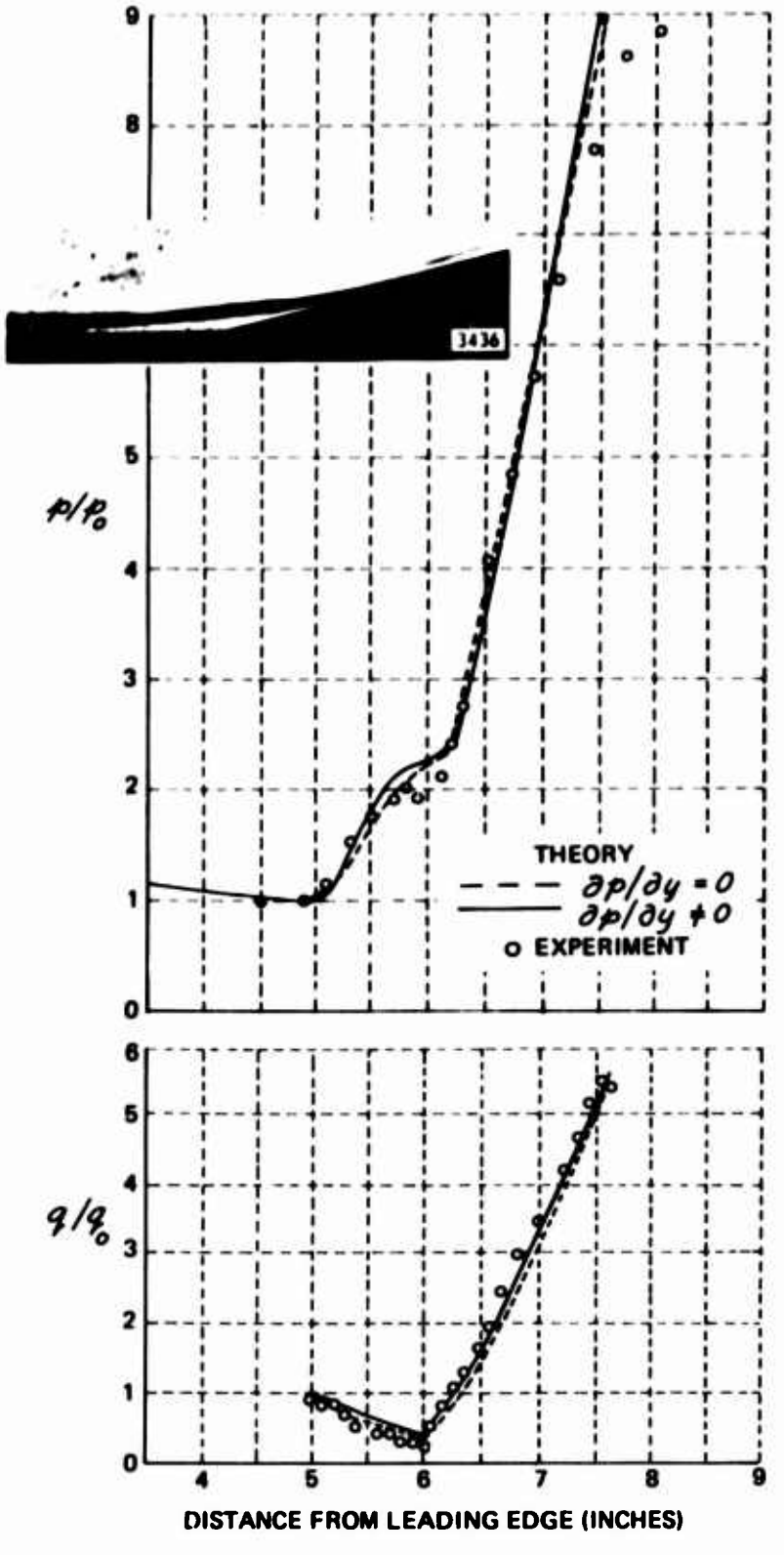

Figure 5 A COMPARISON BETWEEN THEORY AND MEASUREMENTS OF PRESSURE AND HEAT TRANSFER

($M_\infty = 10$, $Re_L = 8.1 \times 10^5$, $\theta_w = 12.5^o$)

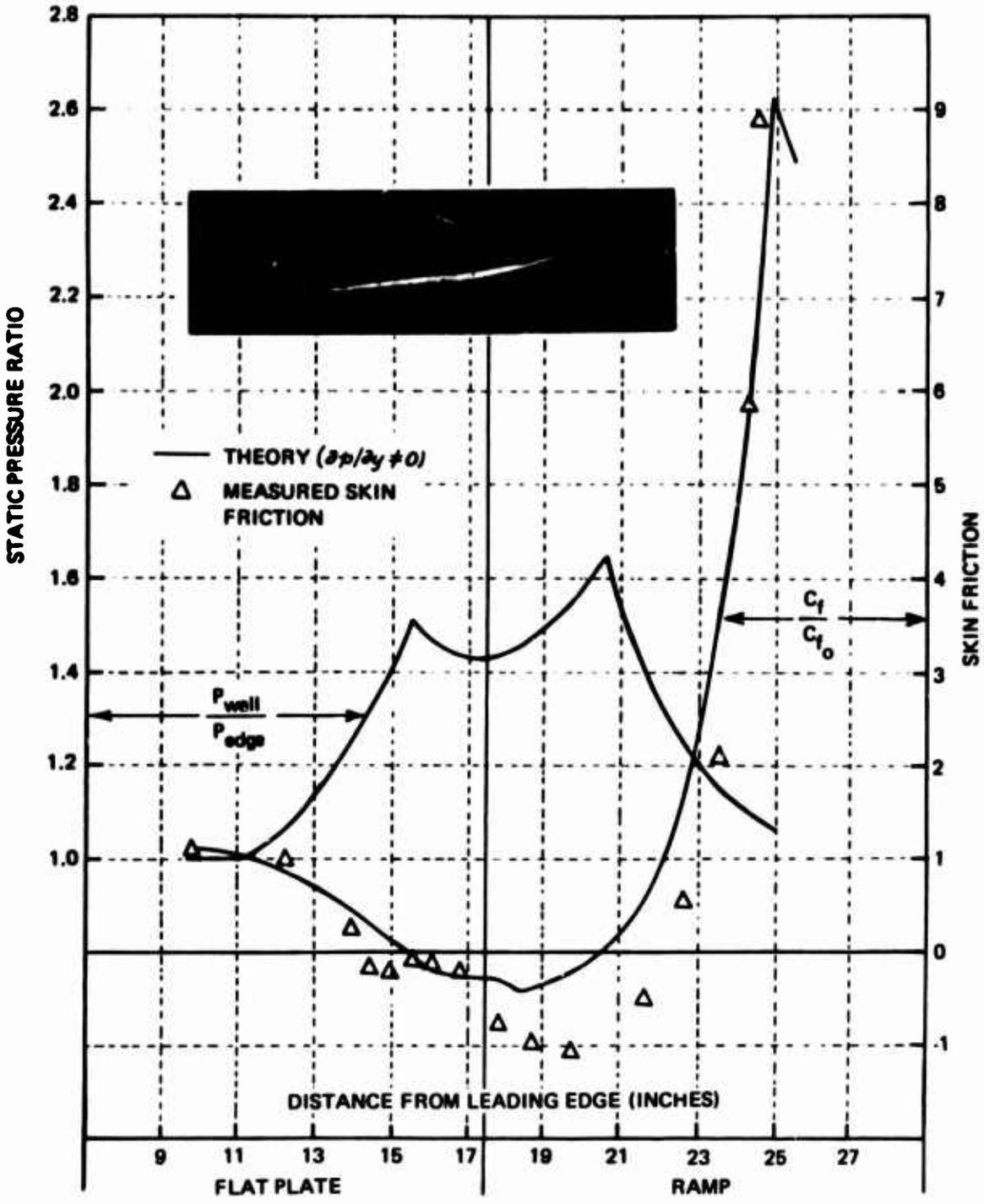

Figure 6a STATIC PRESSURE RATIO AND COMPARISON BETWEEN THEORY AND SKIN FRICTION MEASUREMENTS

($M_\infty = 14.5$, $Re/FT = 1.8 \times 10^5$, $\theta_w = 18^o$)

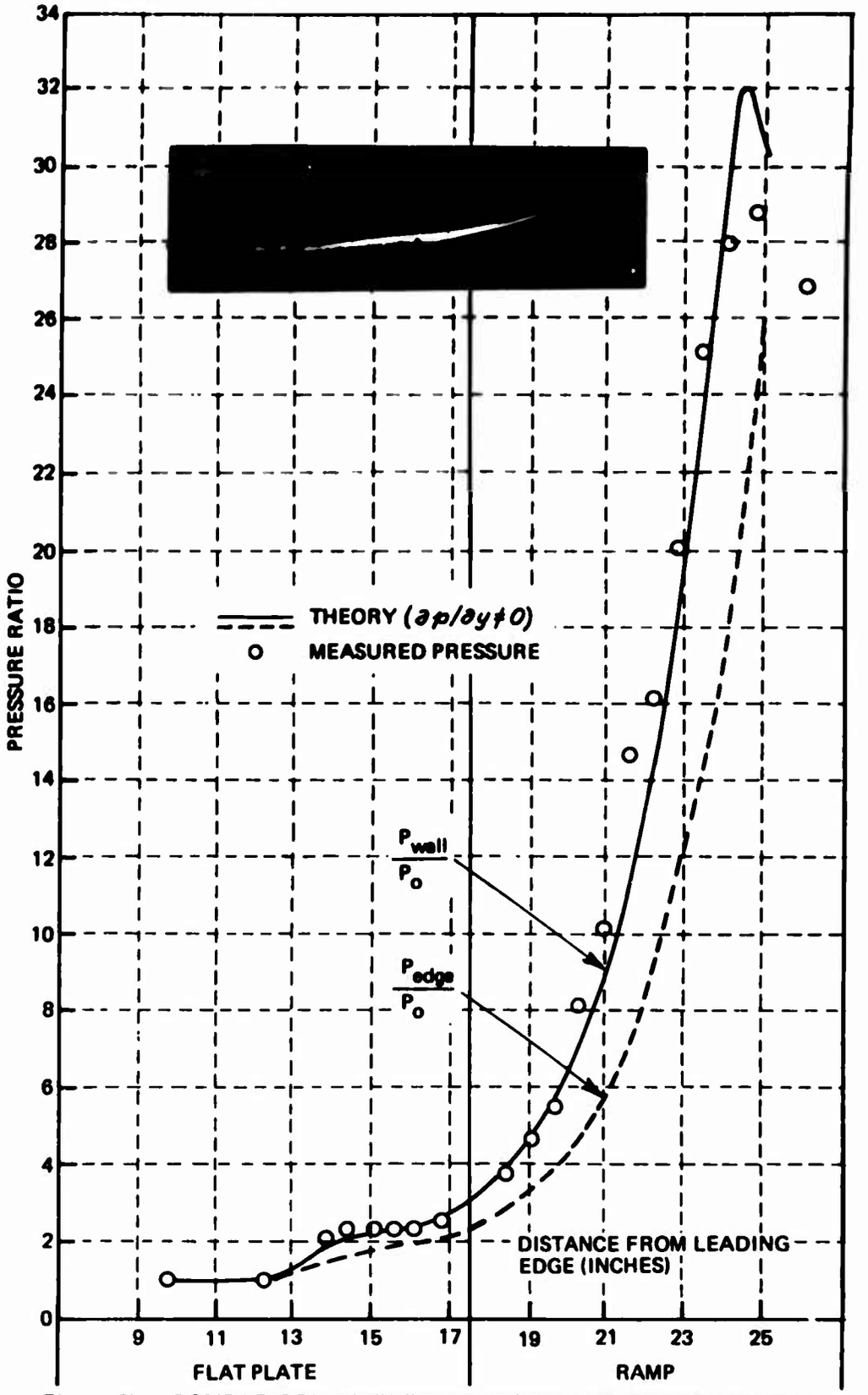

Figure 6b COMPARISON BETWEEN THEORY AND EXPERIMENTAL PRESSURE MEASUREMENTS

($M_\infty = 14.5$, $Re/FT = 1.8 \times 10^5$, $\theta_w = 18^o$)

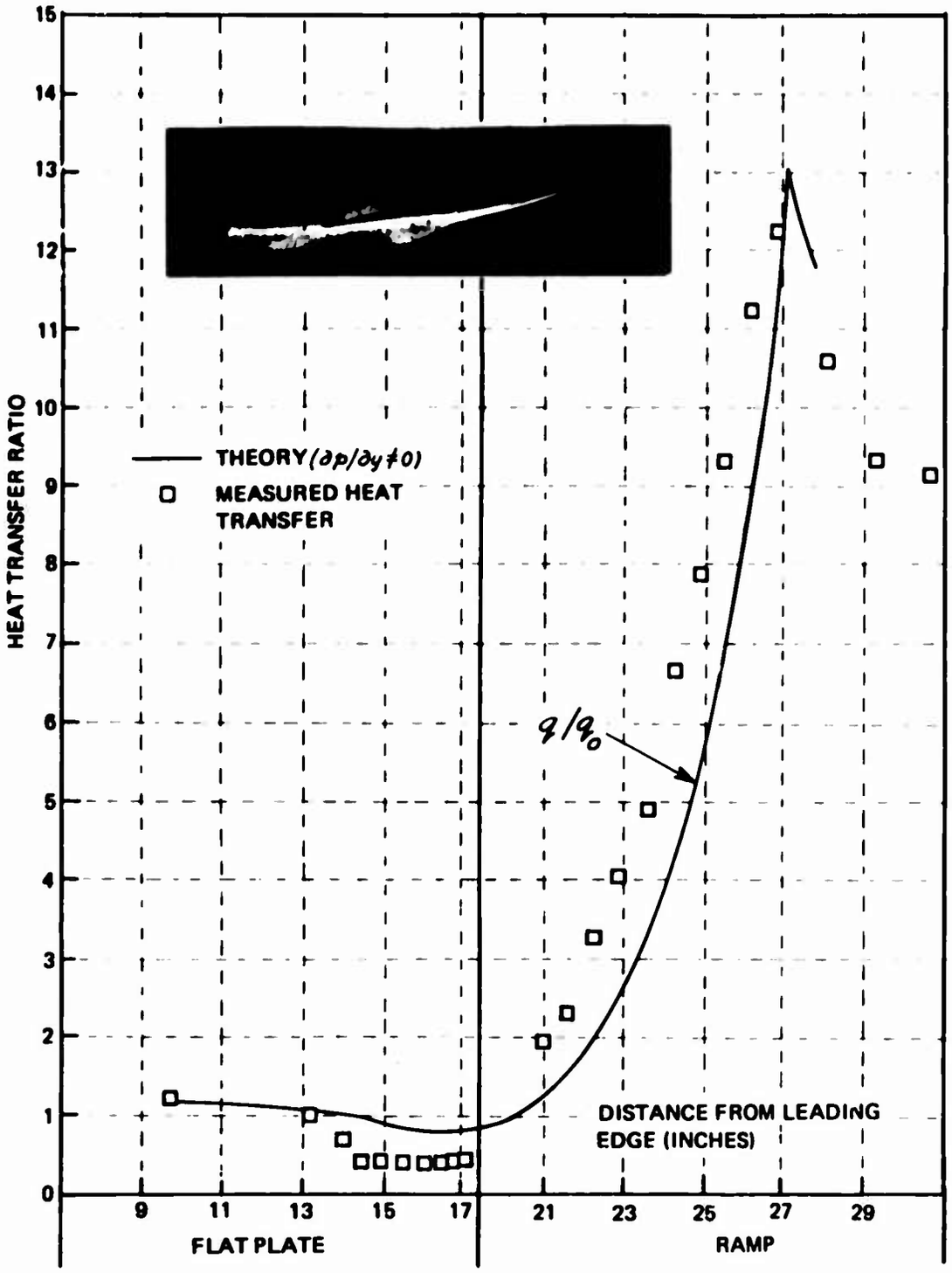

Figure 6c COMPARISON BETWEEN THEORY AND EXPERIMENTAL HEAT TRANSFER MEASUREMENT

(M_∞ = 14.5, Re/FT = 1.8 x 10^5, θ_w = 18^o)

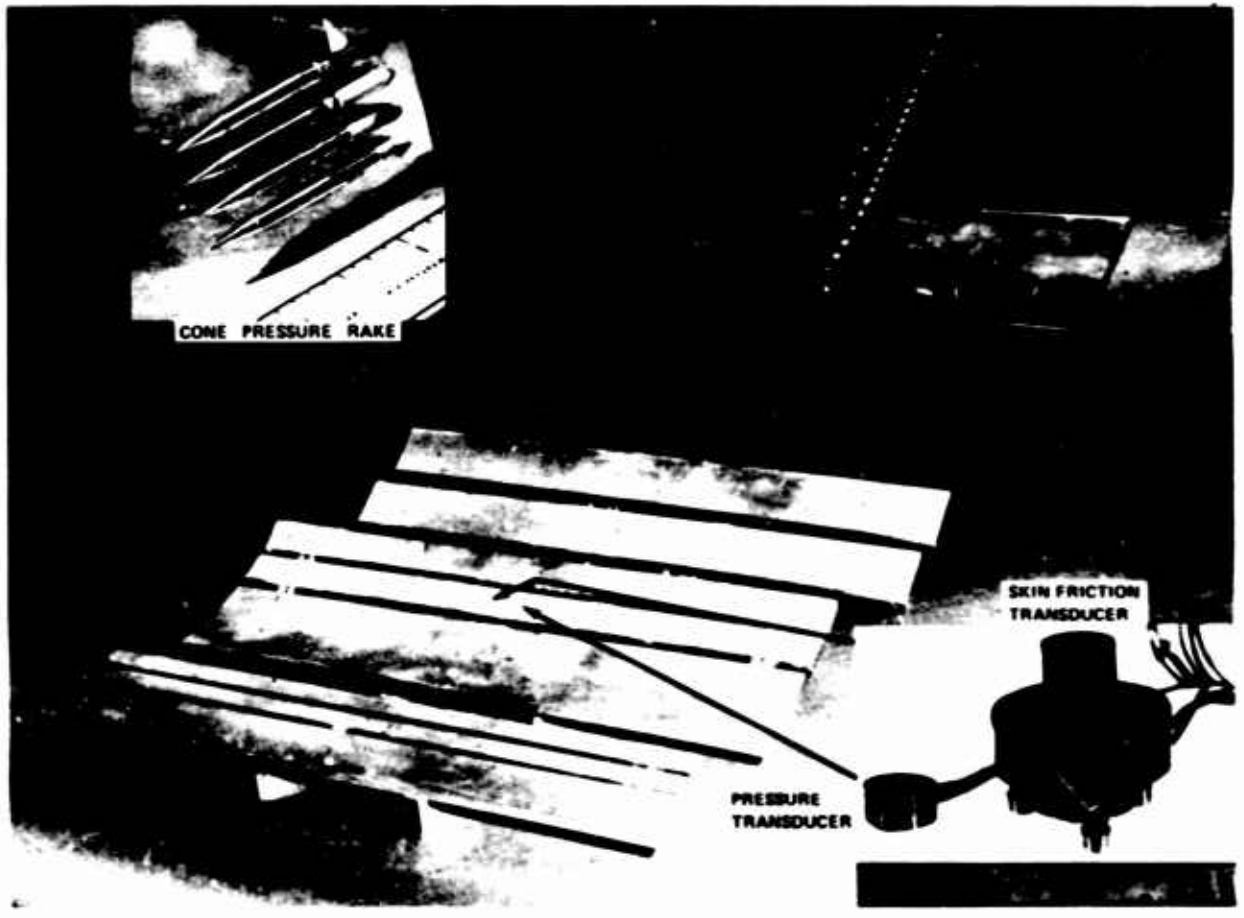

Figure 7 COMPRESSION SURFACE MODEL AND INSTRUMENTATION

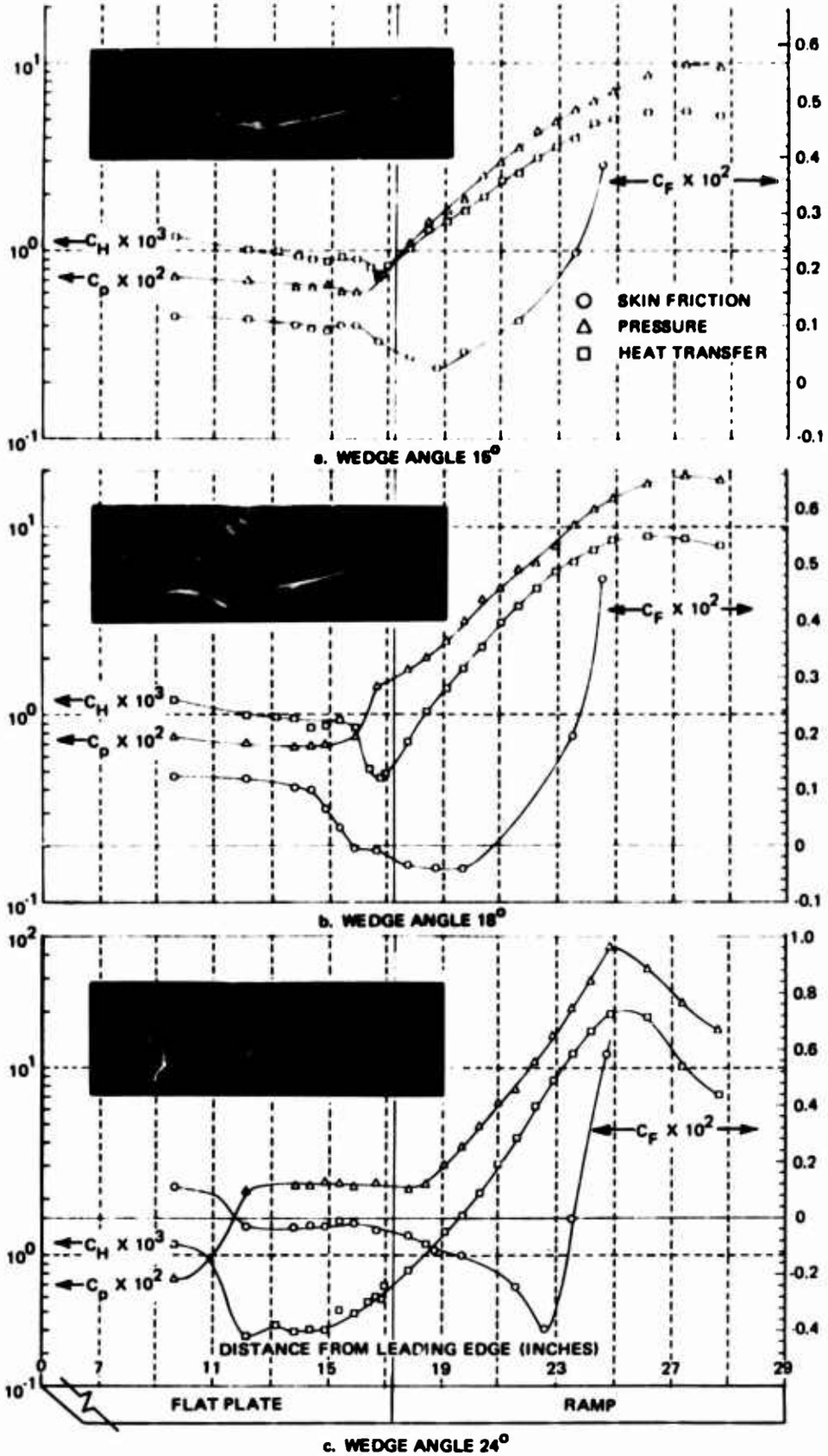

Figure 8 SKIN FRICTION, HEAT TRANSFER, AND PRESSURE DISTRIBUTIONS ON THE FLAT PLATE - WEDGE MODELS

(M_∞ = 14.1, Re/FT = 7.2 x 10^4)

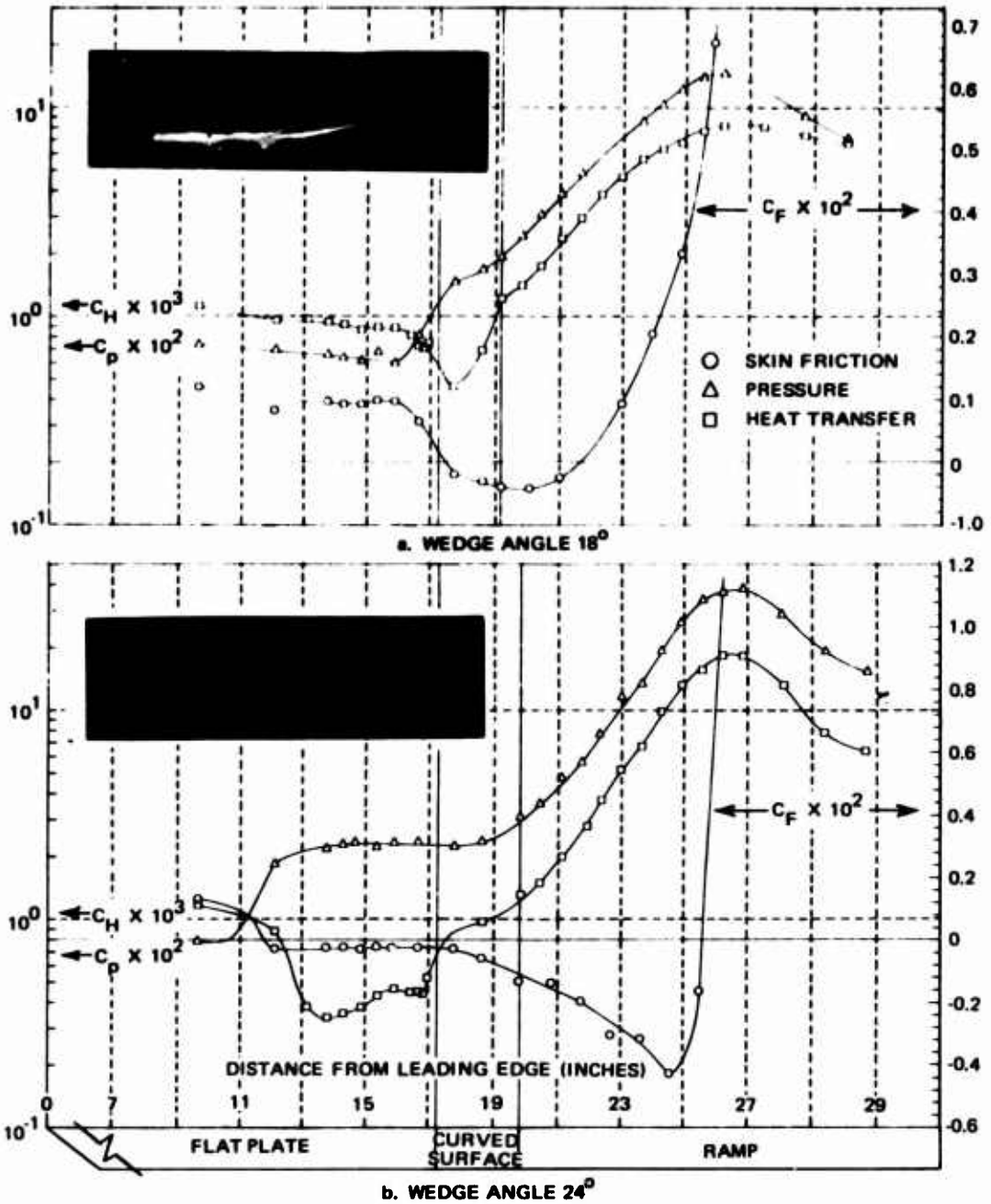

a. WEDGE ANGLE 18°

b. WEDGE ANGLE 24°

Figure 9 SKIN FRICTION, HEAT TRANSFER AND PRESSURE DISTRIBUTIONS ON THE FLAT PLATE - 6"R CYLINDRICAL ARC-WEDGE MODELS (M_∞ = 14.1, Re/FT = 7.2 x 10^4)

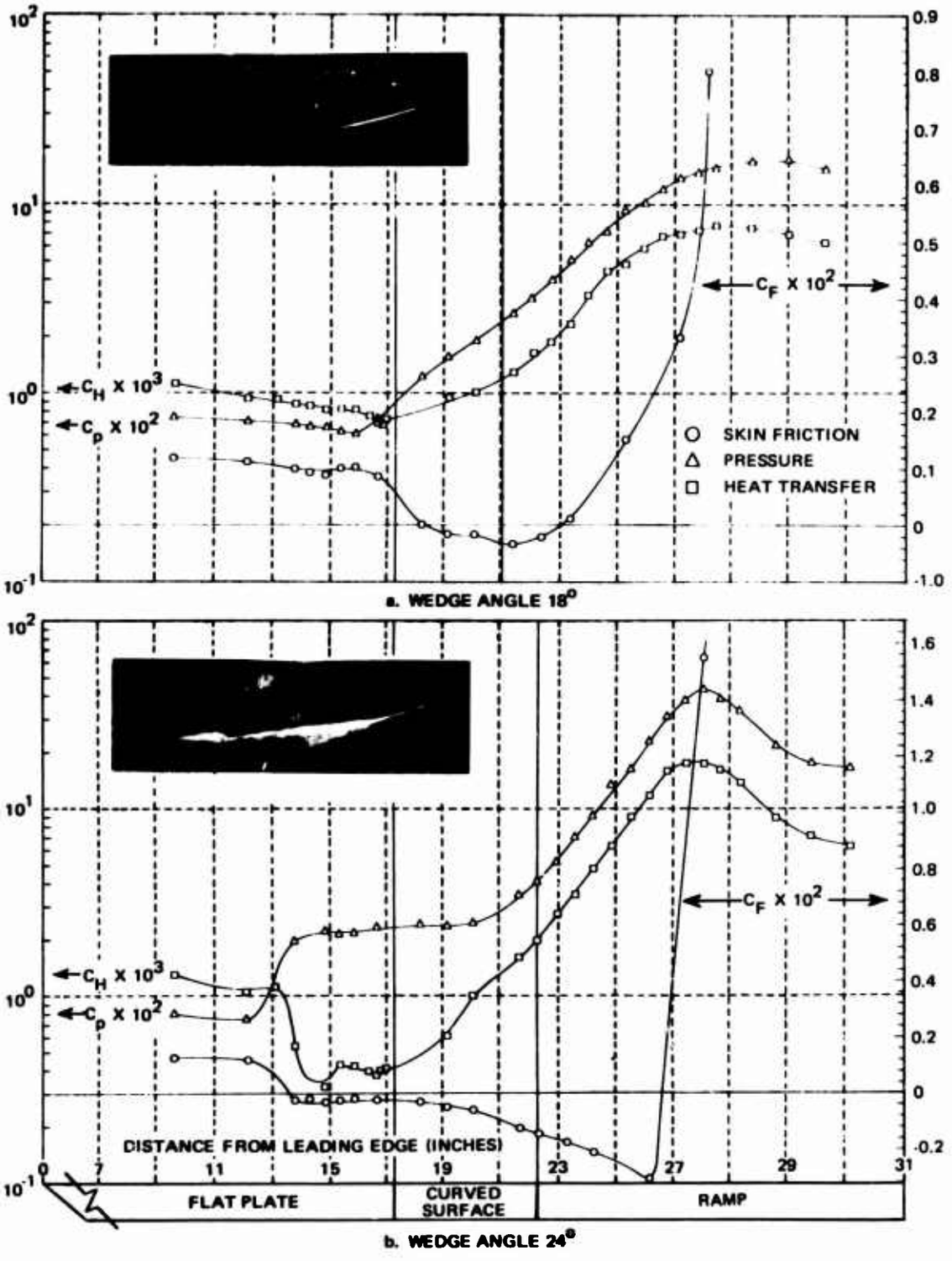

Figure 10 SKIN FRICTION, HEAT TRANSFER AND PRESSURE DISTRIBUTIONS ON THE FLAT PLATE - 12"R CYLINDRICAL ARC-WEDGE MODELS (M_∞ = 14.0, Re/FT = 7.0×10^4)

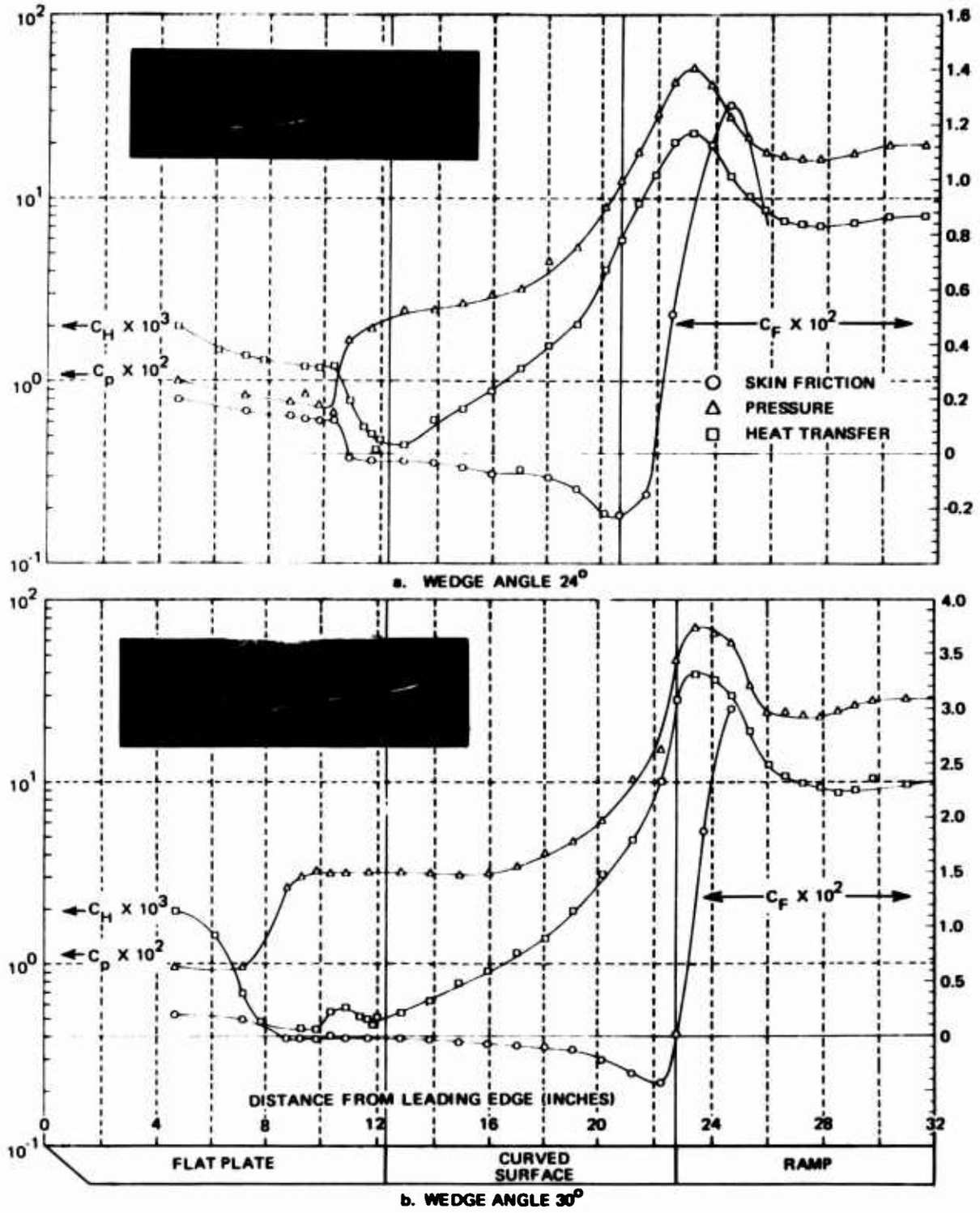

Figure 11 SKIN FRICTION, HEAT TRANSFER AND PRESSURE DISTRIBUTIONS ON THE FLAT PLATE - 20"R CYLINDRICAL ARC-WEDGE MODELS (M_∞ = 14.0, Re/FT = 7.2 x 10^4)

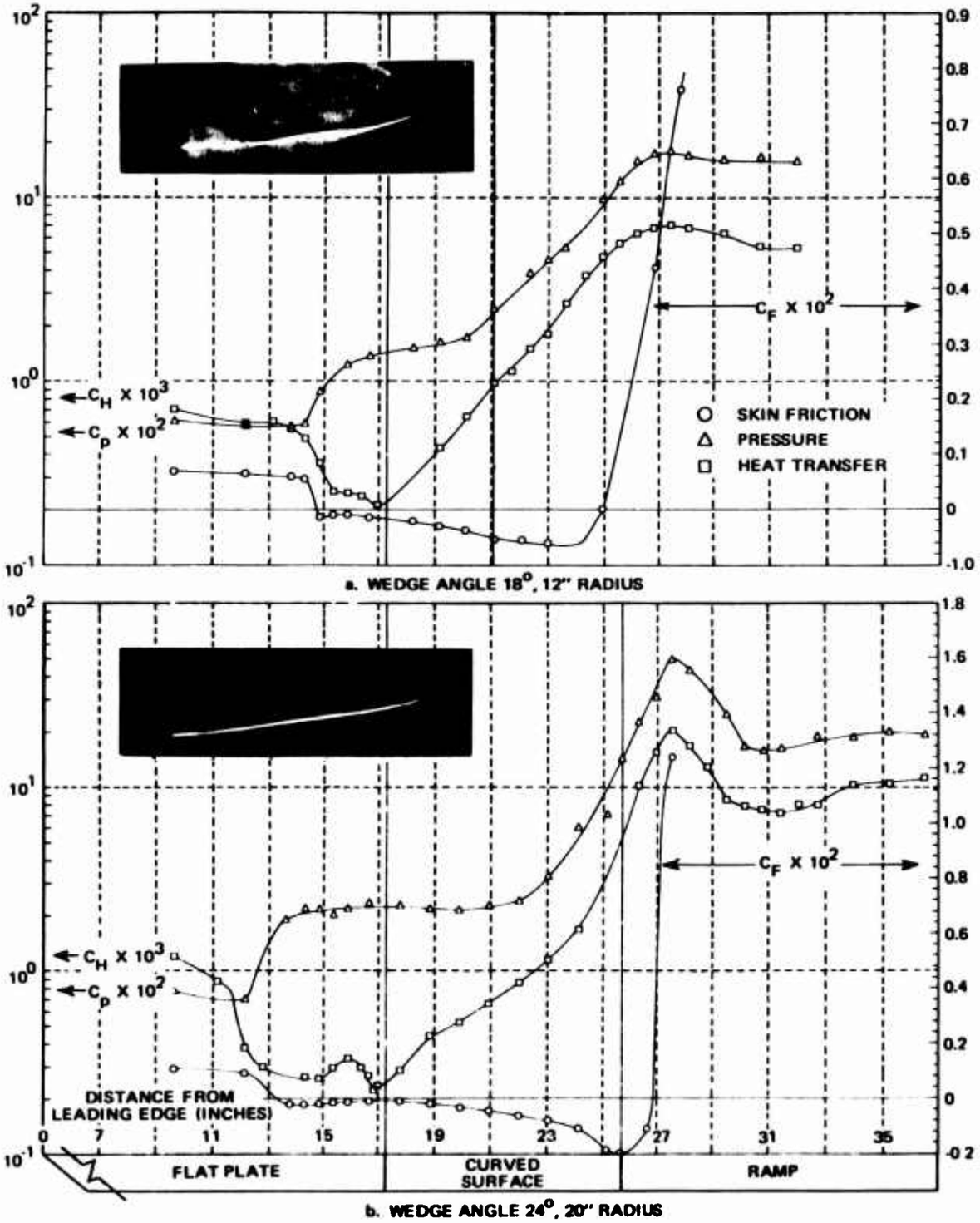

Figure 12 SKIN FRICTION, HEAT TRANSFER AND PRESSURE DISTRIBUTIONS ON THE FLAT PLATE - CYLINDRICAL ARC-WEDGE MODELS (M_∞ = 14.5, Re/FT = 1.8 x 10^5)

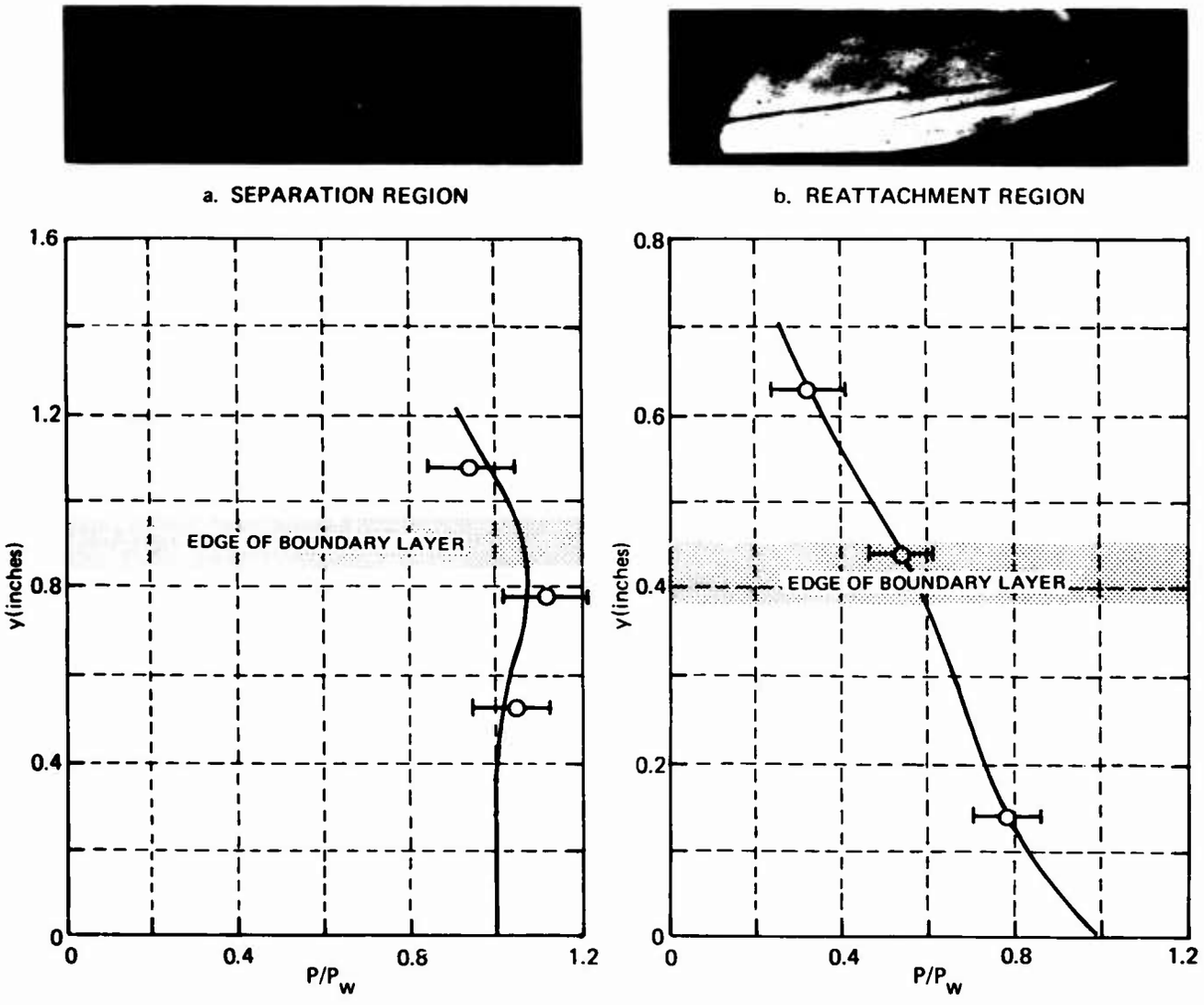

Figure 13 STATIC PRESSURE MEASUREMENTS ACROSS THE BOUNDARY LAYER

(M_∞ = 14.5, Re/FT = 1.8 x 10^5, θ_w = 18°)

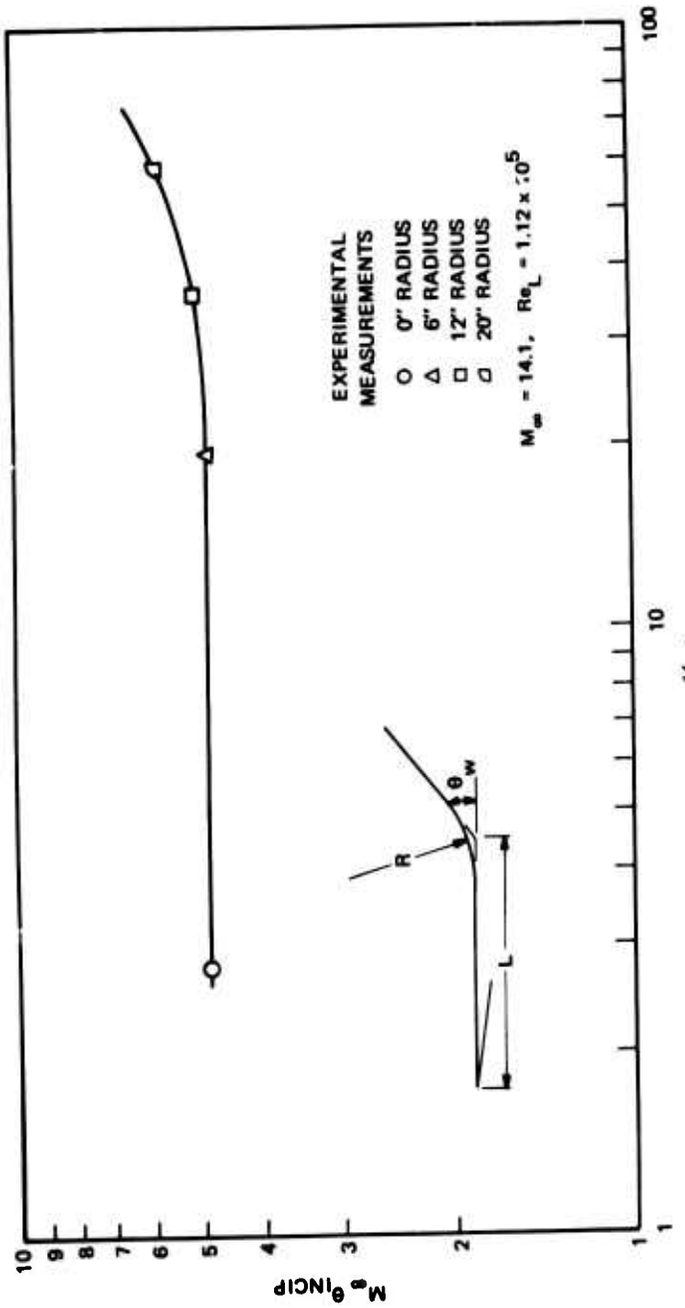

Figure 14 INCIPIENT SEPARATION CONDITIONS FOR CURVED SURFACES

UNCLASSIFIED
Security Classification

DOCUMENT CONTROL DATA - R & D

(Security classification of title, body of abstract and indexing annotation must be entered when the overall report is classified)

1. ORIGINATING ACTIVITY (Corporate author)	2a. REPORT SECURITY CLASSIFICATION
Cornell Aeronautical Laboratory, Inc. Buffalo, New York 14221	Unclassified 2b. GROUP

3. REPORT TITLE

THEORETICAL AND EXPERIMENTAL STUDIES OF THE SHOCK WAVE-BOUNDARY LAYER INTERACTION ON COMPRESSION SURFACES IN HYPERSONIC FLOW

4. DESCRIPTIVE NOTES (Type of report and inclusive dates)

Scientific. Final. November 1966 to November 1969

5. AUTHOR(S) (First name, middle initial, last name)

Michael S. Holden

6. REPORT DATE	7a. TOTAL NO. OF PAGES	7b. NO. OF REFS
January 1970	72	39

8a. CONTRACT OR GRANT NO.	9a. ORIGINATOR'S REPORT NUMBER(S)
F33615-67-C-1298	AF-2410-A-1
b. PROJECT NO. 7064	
c. DoD Element 61102F	9b. OTHER REPORT NO(S) (Any other numbers that may be assigned this report)
d. DoD Subelement 681307	ARL 70-0002

10. DISTRIBUTION STATEMENT

This document has been approved for public release and sale; distribution is unlimited.

11. SUPPLEMENTARY NOTES	12. SPONSORING MILITARY ACTIVITY
TECH OTHER	Aerospace Research Laboratories (ARR) Wright-Patterson AFB, Ohio 45433

13. ABSTRACT The report first summarizes the studies conducted under this contract. A detailed description is then given of the theoretical and experimental studies of shock wave-laminar boundary layer interaction on curved compression surfaces in hypersonic flow. In the theoretical study we have used the integral forms of the boundary layer equations for the conservation of mass, streamwise momentum, normal momentum, moment of streamwise momentum and energy to describe the development of attached and separated boundary layers on a curved surface. In this formulation we do not assume the pressure to be constant across the boundary layer. The theory, which was in good agreement with measurements on compression surfaces in Mach 10 and 14.8 airflows, showed that large pressure gradients can be generated across the boundary layer in the separation and reattachment regions. In the experimental study skin friction, heat transfer and pressure measurements were made on a series of flat plate-cyclindrical arc-wedge compression surfaces. Pitot and cone pressure measurements were made above the surface in the separation and reattachment regions of separated flows to estimate the static pressure difference across the boundary layer. The radius of curvature of the cylindrical arc, the inclination of the wedge, and the unit Reynolds number of the free-stream were varied to examine their effect on the properties of both attached and separated interaction regions over the models. We found that separation first occurred on the compression surface downstream of the flat plate, and incipient separation could not always be detected by observing the first occurrence of an inflexion point in the pressure distribution. The conditions under

DD FORM 1 NOV 68 1473

(Continuation sheet)

UNCLASSIFIED
Security Classification

UNCLASSIFIED

Security Classification

14. KEY WORDS	LINK A		LINK B		LINK C	
	ROLE	WT	ROLE	WT	ROLE	WT
boundary layer						
2nd order solution to the boundary layer equations						
separated viscous flows						
heat transfer, skin friction and pressure						
measurements in attached and separated flows						
incipient separation						
leading edge bluntness						
surface curvature effects						
normal pressure gardients						
hypersonic shock tunnel studies						
high Mach number, low Reynolds number flow						

Security Classification

Continuation

which incipient separation occurs were far less sensitive to surface curvature than those observed in earlier experimental studies.